

# Commensurate stacking within confined ultramicropores boosting acetylene storage capacity and separation efficiency

Zhenghui Huang<sup>1</sup>, Kungang Chai<sup>1</sup>, Chengjun Kang<sup>2</sup>, Rajamani Krishna<sup>3</sup> (✉), and Zhaoqiang Zhang<sup>2</sup> (✉)

<sup>1</sup> Guangxi Key Laboratory of Petrochemical Resource Processing and Process Intensification Technology, School of Chemistry and Chemical Engineering, Guangxi University, Nanning 530004, China

<sup>2</sup> Department of Chemical and Biomolecular Engineering, National University of Singapore, Singapore 117585, Singapore

<sup>3</sup> Van't Hoff Institute for Molecular Sciences, University of Amsterdam, Park 904, Amsterdam 1098 XH, The Netherlands

© The Author(s) 2023

Received: 27 September 2022 / Revised: 5 November 2022 / Accepted: 20 November 2022

## ABSTRACT

Developing advanced porous materials possessing both a high storage capacity and selectivity for acetylene ( $C_2H_2$ ) remains challenging but a sought-after endeavor. Herein we show a strategy involving synergic combination of spatial confinement and commensurate stacking for enhanced  $C_2H_2$  storage and capture via maximizing the host–guest and guest–guest interactions. Two ultramicroporous metal-organic frameworks (MOFs), MIL-160 and MOF-303 are elaborately constructed to exhibit ultrahigh  $C_2H_2$  uptakes of 235 and 195  $cm^3 \cdot g^{-1}$ , respectively, due to the confinement effect of the suitable pore sizes and periodically dispersed molecular recognition sites. Specially,  $C_2H_2$  capacity of MIL-160 sets a new benchmark for  $C_2H_2$  storage. The exceptional separation performances of two materials for  $C_2H_2$  over both  $CO_2$  and ethylene ( $C_2H_4$ ), which is rarely observed, outperform most of the benchmark materials for  $C_2H_2$  capture. We scrutinized the origins of ultrahigh  $C_2H_2$  loading in the confined channels via theoretical investigations. The superior separation efficiency for  $C_2H_2/CO_2$  and  $C_2H_2/C_2H_4$  mixtures with unprecedented  $C_2H_2$  trapping capacity ( $> 200 L \cdot kg^{-1}$ ) was further demonstrated by dynamic breakthrough experiments.

## KEYWORDS

adsorption and separation, acetylene storage, commensurate stacking, gas cluster, metal-organic frameworks

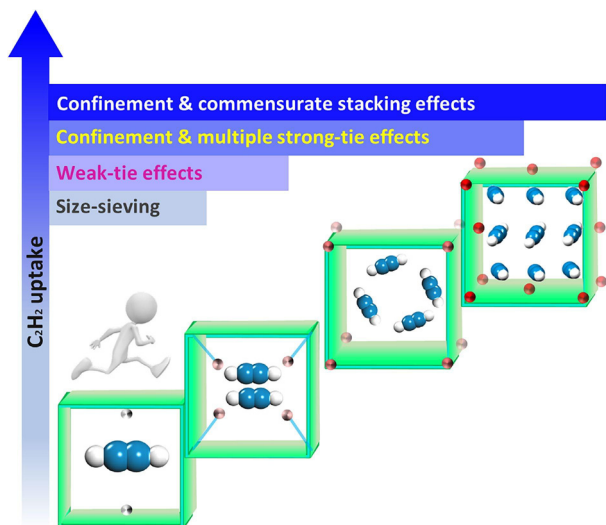
## 1 Introduction

Isolation of acetylene ( $C_2H_2$ ) from various mixtures, especially  $CO_2$  and ethylene ( $C_2H_4$ ) mixtures, is significant for the production of grade A  $C_2H_2$  (content of impurities no more than 0.5%) and high-purity  $C_2H_4$ , which are basic raw materials for a variety of essential chemicals [1–4]. Industrially, the manufacturing processes of  $C_2H_2$  mainly involve partial combustion of natural gas and thermal cracking of hydrocarbons, which inevitably generate by-products, such as  $CO_2$  or  $C_2H_4$  [5, 6]. Furthermore, for  $C_2H_4$  production,  $C_2H_2$  usually co-exists as an impurity, which can poison the catalysts during  $C_2H_4$  polymerization and lower the quality of polyethylene. In these contexts, it is vital but challenging to separate  $C_2H_2$  from the  $CO_2$  or  $C_2H_4$  co-existed crude products due to the similarities of their molecular sizes and physical properties. Compared to the dominant technologies (e.g., absorption and cryogenic distillation), adsorptive separation has presented as a promising alternative process for  $C_2H_2$  purification and capture with low energy consumption [7–9]. The key factor that guarantees the high performance of this sustainable and energy-efficient separation technology, is designing suitable adsorbents that can preferentially adsorb  $C_2H_2$  over other gases with ultrahigh capacity and selectivity, however, it is a nontrivial task.

The emergence of metal-organic frameworks (MOFs) or porous coordination polymers, self-assembled through the coordination of metal nodes to organic linkers, has triggered

extensive researches to optimize the performance for selective capture of  $C_2H_2$  [1, 10–12]. MOFs have gained a reputation as promising candidates for  $C_2H_2$  trapping due to the inherent features of structural diversity, tunable porosity, and tailorable functionality or pore chemistry [13–16]. The introduction of unsaturated open metal sites (OMSs) and other functional sites in MOFs has been extensively investigated to strengthen the affinity for  $C_2H_2$ , but only moderate  $C_2H_2$  selectivity and capacity were achieved (Scheme 1) [17–26]. Fine tuning of the pore size provides the possibility to sieve  $C_2H_2$  from the larger  $C_2H_4$  molecule (Table S1 in the Electronic Supplementary Material (ESM)) [1, 17, 27–29]. However, the exploitation of the size-sieving materials is a daunting challenge, and the  $C_2H_2$  adsorption capacity is still moderate due to the limited pore volume. For example, UTSA-200 can sieve  $C_2H_2$  from  $C_2H_4$ , but the capacity is only 116  $cm^3 \cdot g^{-1}$ . Thus, the trade-off effect between the uptake and selectivity for  $C_2H_2$  unavoidably poses great challenges for the discovery of novel advanced porous materials in the  $C_2H_2$  related separation processes.

Ultramicroporous MOFs (pore size  $< 0.7$  nm) have been envisaged as a suitable platform to pursue promising materials for  $C_2H_2$  capture [30]. The suitable ultramicropore is supposed to provide a well confined environment for accommodation of multiple  $C_2H_2$  molecules and occurrence of the maximization of host–guest and guest–guest interactions, thus enhancing the  $C_2H_2$  uptake. Great endeavors have been made to develop tailor-made



**Scheme 1** Schematic representation of various mechanisms for  $C_2H_2$  capture within porous materials.

MOFs for  $C_2H_2$  capture [3, 31–39], and a high degree of controlling the oriented arrangement regarding the recognition sites and the spatial confinement behavior were proved to be beneficial for the formation of  $C_2H_2$  clusters, then leading to high  $C_2H_2$  capacity. A prominent example is SIFSIX-1-Cu, which possesses high  $C_2H_2$  capacity ( $190.4 \text{ cm}^3\text{g}^{-1}$ ) and good  $C_2H_2/C_2H_4$  (50/50) separation selectivity due to the fact that  $C_2H_2$  molecules formed “gas clusters” through intermolecular guest–guest interactions within the confined pores (Scheme 1) [22]. However, the potential use of SIFSIX-1-Cu for industrial  $C_2H_2/C_2H_4$  separation was hampered by its intrinsic features of high cost and low operational stability. Nevertheless, the principle mentioned above opened a powerful approach for solving the trade-off problem. Bearing this in mind, CAU-10-H and CAU-10- $NH_2$  were reported with an appropriate functionalized pore environment to enable efficient  $C_2H_2$  packing, however, the  $C_2H_2$  uptakes ( $89.8$  and  $105.3 \text{ cm}^3\text{g}^{-1}$ , respectively) are still moderate [40, 41]. Furthermore, to our knowledge, the development of one material that can simultaneously separate  $C_2H_2/C_2H_4$  and  $C_2H_2/CO_2$  with high efficiency, is rarely reported and still remains a challenge as the above cases merely focused on the separation of either  $C_2H_2/C_2H_4$  or  $C_2H_2/CO_2$  mixture. To break the current bottleneck for boosting  $C_2H_2$  adsorption capacity and selectivity within the confined ultramicropores, exploration of novel adsorption mechanism regarding such as expansion of  $C_2H_2$  cluster by reinforcing the multiple host–guest and guest–guest interactions is highly desirable.

Herein, we exquisitely integrate the pore confinement and commensurate stacking mechanism into the tailor-made MOFs for  $C_2H_2$  capture with ultrahigh capacity (Scheme 1). To exemplify this strategy, two aluminum-based MOFs, MIL-160, and MOF-303 with one-dimensional (1D) ultramicroporous channels were constructed with periodically dispersed electronegative binding sites on the pore surfaces. Especially, the commensurate stacking of  $C_2H_2$  along the channel axis in MIL-160 was observed to afford a record-high  $C_2H_2$  uptake of  $235 \text{ cm}^3\text{g}^{-1}$  at 298 K and 1 bar, equal to 9 molecules of  $C_2H_2$  per cell, enabling MIL-160 to outperform the benchmark materials. The specific commensurate stacking and guest–guest interactions between  $C_2H_2$  were verified via molecular simulations. Encouragingly, these two MOFs exhibited simultaneously for both equimolar  $C_2H_2/CO_2$  and  $C_2H_2/C_2H_4$  mixtures. Additionally, MIL-160 and MOF-303 showed excellent stability and can be rapidly obtained via microwave synthesis using cheap materials. In this contribution, not only the perfect

match of multiple binding sites for  $C_2H_2$  and pore confinement were realized within the model MOFs, but also the separation potential for industrial applications was demonstrated via dynamic separation process.

## 2 Results and discussion

MIL-160 and MOF-303 are constructed using  $AlCl_3 \cdot 6H_2O$  and two bent dicarboxylic linkers, 2,5-furandicarboxylic acid (FDC) and 3,5-pyrazoledicarboxylic acid (PZDC), respectively (Fig. 1(a)), via the microwave synthesis method. In order to better activate the pore channel, the two MOFs were treated by methanol exchange for three times. MIL-160 exhibits yfm topology and is constructed by fourfold helical rod-like secondary building units (SBUs) of cis-corner sharing  $AlO_6$  polyhedra bridged by FDC linkers (Fig. 1(b)). Besides, MOF-303 with xhh topology is built from infinite  $Al(OH)(-COO)_2$  SBUs consisting of alternating cis-trans corner-shared  $AlO_6$  octahedra that are connected by PZDC linkers (Fig. 1(c)). The overall three-dimensional (3D) structures of two materials are found to be ultramicroporous in nature having a square-shaped channel with dimension  $5.0 \text{ \AA} \times 5.0 \text{ \AA}$  for MIL-160 and a pseudo-square channel of dimension  $5.8 \text{ \AA} \times 5.9 \text{ \AA}$  for MOF-303. The ultramicroporous feature can provide well confined environment for gas molecules. Particularly, the strategic adoption of the electronically polarized five-membered O,N-heterocycles ligands with additional functionalities, such as furan oxygens and N-termini of pyrazole groups, provides multiple potential electronegative binding sites for gas molecules. The periodical arrangement of these heteroatoms, akin to the quadrangle configuration of F atoms in SIFSIX-1-Cu pore channels, is in favor of maximizing the host–guest interactions and forming gas clusters through guest–guest interactions. Furthermore, combining the suitable pore dimension, such a regular layout of pore environment would favor the commensurate stacking of gas molecules.

Experimentally, the crystallinity and phase purity of the synthesized MIL-160 and MOF-303 were first investigated by powder X-ray diffraction (PXRD) (Figs. S1–S3 in the ESM). The sharp diffraction peaks match well with the simulated diffraction patterns for both MIL-160 and MOF-303, verifying the high crystallinity and phase purity. Besides, the permanent porosity of two materials was investigated by  $N_2$  adsorption–desorption isotherms at 77 K (Fig. S4 in the ESM). Two materials exhibited

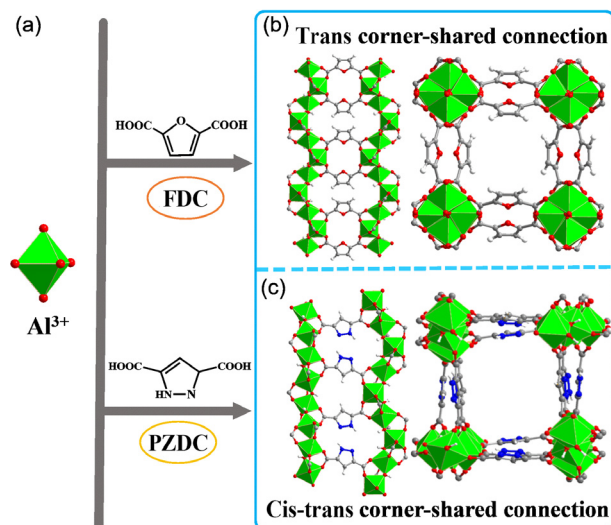


**Figure 1** (a) Self-assembly of MIL-160 and MOF-303. Crystal structures of (b) MIL-160 and (c) MOF-303. The  $AlO_6$  polyhedra is shown in green, the O atom is shown in red, the H atom is shown in white, and the C atom is shown in gray.

typical type-I adsorption behaviors, indicating the ultramicropores in the frameworks (Table S2 and Fig. S5 in the ESM). The Brunauer–Emmett–Teller (BET) surface areas of MIL-160 and MOF-303 were calculated to be 1110 and 1343  $\text{m}^2\cdot\text{g}^{-1}$ , respectively, which were consistent with the previously reported values (Table S2 in the ESM). Further, the PXRD patterns as well as the  $\text{N}_2$  adsorption–desorption isotherms of MIL-160 and MOF-303 remained intact after immersing in water for one week (Figs. S6 and S7 in the ESM), demonstrating no phase transitions and porous structure collapse occurred. The excellent stability is highly desirable in industrial process.

The confined pore environments imparted by combining suitable ultramicropores with periodically dispersed molecular recognition sites of the model MOFs prompt us to explore their potential for  $\text{C}_2\text{H}_2$  capture and purification. To begin with, the single-component adsorption isotherms of  $\text{C}_2\text{H}_2$ ,  $\text{C}_2\text{H}_4$ , and  $\text{CO}_2$  on MIL-160 and MOF-303 were collected under different temperatures (Figs. 2(a) and 2(b) and Figs. S8–S11 in the ESM). Before each test, the samples were immersed in methanol and activated at 393 K for 12 h. Surprisingly, MIL-160 and MOF-303 exhibit the ultrahigh  $\text{C}_2\text{H}_2$  uptakes of 235 and 195  $\text{cm}^3\cdot\text{g}^{-1}$ , respectively, at 298 K and 1.0 bar. The  $\text{C}_2\text{H}_2$  uptake on MIL-160 is much higher than the reported values by Li and Ma [42] (Fig. S30 in the ESM), which is resulted from the well-activated pore channels, and the  $\text{C}_2\text{H}_2$  uptake exceeds the top-performing materials reported so far (Fig. 2(c) and Fig. S12 in the ESM), such as the typically OMS-type MOFs of FJU-H8 (224  $\text{cm}^3\cdot\text{g}^{-1}$ ) [18], co-MOF-74 (197  $\text{cm}^3\cdot\text{g}^{-1}$ ) [20], and ZJU-5 (193  $\text{cm}^3\cdot\text{g}^{-1}$ ) [21]; functionality-type MOFs of SIFSIX-1-Cu (190  $\text{cm}^3\cdot\text{g}^{-1}$ ) [22], ZUL-100 (118.5  $\text{cm}^3\cdot\text{g}^{-1}$ ) [43], and ZNU-1 (76  $\text{cm}^3\cdot\text{g}^{-1}$ ) [44]; and recently-reported SNNU-27 (182.4  $\text{cm}^3\cdot\text{g}^{-1}$ ) [38] and FJU-90 (180  $\text{cm}^3\cdot\text{g}^{-1}$ ) [39]. Obviously, the  $\text{C}_2\text{H}_2$  capacity on MIL-160 sets a new benchmark for porous materials used for  $\text{C}_2\text{H}_2$  storage. Exhilaratingly, MIL-160 and MOF-303 also showed top-performing  $\text{C}_2\text{H}_2$  storage density of 0.63 and 0.43  $\text{g}\cdot\text{cm}^{-3}$  derived from the exceptional  $\text{C}_2\text{H}_2$  uptake and modest pore volume (Fig. 2(d)). To the best of our knowledge, the storage density of MIL-

160 outperforms the second place (lower than MOF-OH) compared to the benchmark MOFs including CAU-10-H (0.392  $\text{cm}^3\cdot\text{g}^{-1}$ ) and CAU-10-NH<sub>2</sub> (0.46  $\text{cm}^3\cdot\text{g}^{-1}$ ) [40, 45], implying that except for  $\text{C}_2\text{H}_2$  clusters in MIL-160 pore channels,  $\text{C}_2\text{H}_2$  molecules may be commensurately stacked or compressed in the confined pore environment.

Detailed analysis of the adsorption properties of  $\text{C}_2\text{H}_2$ ,  $\text{CO}_2$ , and  $\text{C}_2\text{H}_4$  to gain insights into the potential of MIL-160 and MOF-303 for  $\text{C}_2\text{H}_2$  capture, the gas uptake of MIL-160 followed the trend:  $\text{C}_2\text{H}_2$  (235  $\text{cm}^3\cdot\text{g}^{-1}$ ) >  $\text{C}_2\text{H}_4$  (108  $\text{cm}^3\cdot\text{g}^{-1}$ ) >  $\text{CO}_2$  (107  $\text{cm}^3\cdot\text{g}^{-1}$ ), corresponding to 8.7  $\text{C}_2\text{H}_2$ , 3.8  $\text{C}_2\text{H}_4$ , and 3.8  $\text{CO}_2$  per cell (Fig. 2(a)). Such a high trapping number of  $\text{C}_2\text{H}_2$  (ca. 9) in one cell is for the first time observed in ultramicroporous MOFs. Impressively, the  $\text{C}_2\text{H}_2$  isotherm exhibited a steep increase at low pressure regions, whereas the  $\text{C}_2\text{H}_4$  and  $\text{CO}_2$  adsorbed amount grew slowly with the pressure increasing and ultimately formed two similar curves, which may be attributed to the fact that the uniformly arranged electronegative O atoms can provide preferential binding affinity for  $\text{C}_2\text{H}_2$  over  $\text{C}_2\text{H}_4$  and  $\text{CO}_2$ . Besides, the gravimetric gas adsorption amount on MOF-303 followed a sequence of  $\text{C}_2\text{H}_2$  (195  $\text{cm}^3\cdot\text{g}^{-1}$ ) >  $\text{C}_2\text{H}_4$  (118  $\text{cm}^3\cdot\text{g}^{-1}$ ) >  $\text{CO}_2$  (117  $\text{cm}^3\cdot\text{g}^{-1}$ ) under the same conditions, corresponding to 6.9  $\text{C}_2\text{H}_2$ , 4.1  $\text{C}_2\text{H}_4$ , and 4.1  $\text{CO}_2$  per cell (Fig. 2(b)). It is noteworthy that the  $\text{C}_2\text{H}_2$  and  $\text{C}_2\text{H}_4$  curves showed rapid and sharp increases at low pressure regions, while  $\text{CO}_2$  uptake nearly increased linearly with the pressure up to 1.0 bar, suggesting that the dual-nitrogen basic sites in the framework may favor the selective binding of  $\text{C}_2\text{H}_2$  and  $\text{C}_2\text{H}_4$  with acidic H atoms over  $\text{CO}_2$ . Additionally, an overlay of the adsorption and desorption branches with almost no hysteresis on two materials implies that the adsorption process was reversible and the materials can be easily regenerated under mild conditions.

The separation potential of two materials for equimolar binary mixtures of  $\text{C}_2\text{H}_2/\text{CO}_2$  and  $\text{C}_2\text{H}_2/\text{C}_2\text{H}_4$  was evaluated by the ideal adsorbed solution theory (IAST) selectivity (Fig. S13 in the ESM). The selectivities of MIL-160 and MOF-303 at 298 K and 1.0 bar were calculated to be 11 and 10.7 for  $\text{C}_2\text{H}_2/\text{CO}_2$ , 9.7 and 10.8 for

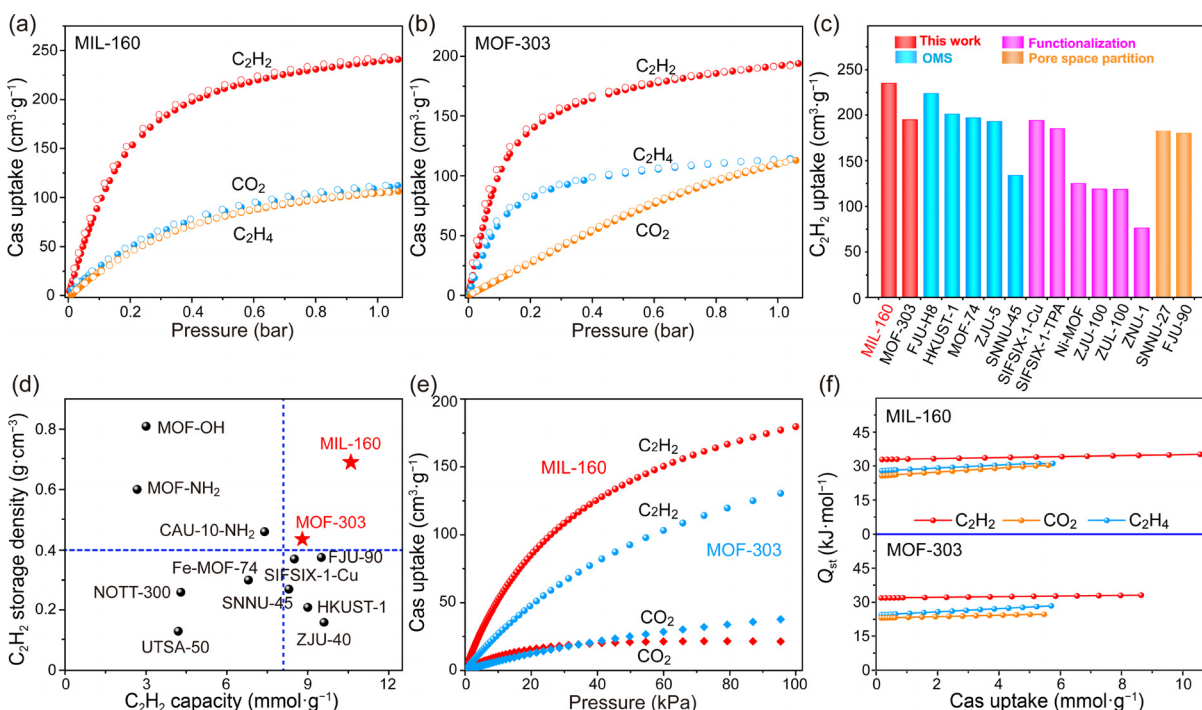


**Figure 2** (a)  $\text{C}_2\text{H}_2$ ,  $\text{CO}_2$ , and  $\text{C}_2\text{H}_4$  adsorption isotherms on MIL-160 at 298 K. (b)  $\text{C}_2\text{H}_2$ ,  $\text{CO}_2$ , and  $\text{C}_2\text{H}_4$  adsorption isotherms on MOF-303 at 298 K. (c) Comparison of  $\text{C}_2\text{H}_2$  uptake on the top-performing materials at 298 K and 1.0 bar. (d) Comparison of the  $\text{C}_2\text{H}_2$  storage density of different MOFs at 298 K and 1.0 bar. (e) Predicted mixture adsorption isotherms of MIL-160 and MOF-303 based on IAST for a 50/50  $\text{C}_2\text{H}_2/\text{CO}_2$  mixture at 298 K. (f) The isosteric  $Q_{st}$  of  $\text{C}_2\text{H}_2$ ,  $\text{CO}_2$ , and  $\text{C}_2\text{H}_4$  for MIL-160 and MOF-303.

$C_2H_2/C_2H_4$ , respectively. Based on IAST calculations, the  $C_2H_2$  uptakes from  $C_2H_2/CO_2$  and  $C_2H_2/C_2H_4$  mixtures can reach  $8.0 \text{ mmol}\cdot\text{g}^{-1}$  (Fig. 2(e) and Fig. S14 in the ESM). The exceptional performance with balanced  $C_2H_2/CO_2$  and  $C_2H_2/C_2H_4$  separation selectivities as well as the ultrahigh  $C_2H_2$  uptake outperformed most materials designed for the separation of  $C_2H_2/CO_2$  and  $C_2H_2/C_2H_4$  mixtures [1, 9, 12, 13, 15, 24, 30]. Thus, with the suitable dimension and molecular recognition sites, MIL-160 not only breaks the record in  $C_2H_2$  uptake capacity, but also strikes an excellent selectivity balance between the two pairs of  $C_2H_2/CO_2$  and  $C_2H_2/C_2H_4$  mixtures.

To decode the high density and selective uptake of  $C_2H_2$  in the two MOFs, the heat of adsorption ( $Q_{st}$ ) for  $C_2H_2$ ,  $CO_2$ , and  $C_2H_4$  was calculated. The  $Q_{st}$  values of MIL-160 and MOF-303 follow the same trend of  $C_2H_2 > C_2H_4 > CO_2$ , indicating the stronger affinity of these two MOFs for  $C_2H_2$  over  $C_2H_4$  and  $CO_2$  (Fig. 2(f)). Meanwhile, MIL-160 and MOF-303 show the modest  $Q_{st}$  values for  $C_2H_2$  with 35.1 and 33.3  $\text{kJ}\cdot\text{mol}^{-1}$ , respectively. These values are obviously lower than that of many well-known MOFs, such as NKMOF-1-Ni (60.3  $\text{kJ}\cdot\text{mol}^{-1}$ ) [14], UTSA-300 (57.6  $\text{kJ}\cdot\text{mol}^{-1}$ ) [1], and SIFSIX-series materials (up to 41.9  $\text{kJ}\cdot\text{mol}^{-1}$ ) [31]. This indicates the model MOFs can achieve a reversible adsorption/desorption process under moderate conditions and afford great reduction in energy intake for adsorbent regeneration. Besides, the  $Q_{st}$  values of  $C_2H_2$  on two MOFs slightly increase with the increasing  $C_2H_2$  uptakes, which hints that the intermolecular interactions contribute an important role in efficiently commensurate stacking of  $C_2H_2$  molecules in the pore channels. This  $C_2H_2$  commensurate stacking phenomenon along with  $Q_{st}$  increase on  $C_2H_2$  adsorption is similar with that in SIFSIX-1-Cu and CAU-10-H-NH<sub>2</sub> [22, 40, 41]. Therefore, the concomitant OMSs-free and commensurate stacking within two Al-MOFs culminated in achieving ultrahigh  $C_2H_2$  storage density but with moderate  $Q_{st}$  values of  $C_2H_2$ .

To delve deeper into the underlying mechanism for the ultrahigh  $C_2H_2$  capacity and separation performance, grand canonical Monte Carlo (GCMC) simulations and density

functional theory (DFT) calculations were conducted because the single crystals of Al-MOFs could not be obtained. The results show that the large  $C_2H_2$  clusters with 9 and 7  $C_2H_2$  molecules are accommodated in the unit cells of MIL-160 and MOF-303, respectively (Figs. 3(a) and 3(d)). The values are consistent with the captured  $C_2H_2$  numbers (8.7 and 6.9) by each unit cell calculated from the adsorption isotherms. Notably, two distinct ordered  $C_2H_2$  arrangements (parallel and staggered) resulted from the strong host-guest and guest-guest interactions were observed in the open pores of MIL-160 and MOF-303 (Figs. S21 and S22 in the ESM). The previous work of MIL-160 only showed the host-guest interaction between one  $C_2H_2$  and the host framework [42], but the true nature for high  $C_2H_2$  uptake was not legitimately provided. In this work, such a unique commensurate stacking mechanism with host-guest and guest-guest interactions was for the first observed in MOFs for light hydrocarbon (C1-C4) adsorption. This implies that the fine-tuning of pore spacing and binding sites arrangement in confined pore channels play paramount roles in the organization of  $C_2H_2$  molecules within MOFs (Tables S5–S8 in the ESM).

Apparently, the occurrence of multiple host-guest interactions is observed on two materials (Figs. 3(a) and 3(d)). Besides the  $C-H^{\delta+}\cdots O^{\delta-}$  and  $C-H^{\delta+}\cdots N^{\delta-}$  interactions (ranging from 2.819 to 3.632 Å) between  $C_2H_2$  molecule and the electronegative O and N atoms from the carboxylate group, furan, and pyrazole units, the host-guest interactions are also supplemented by parallel  $\pi\cdots\pi$  interactions between the  $\pi$ -electrons of  $C_2H_2$  and furan (pyrazole) rings. In addition, there exists one  $C_2H_2$  molecule being fully surrounded by other  $C_2H_2$  molecules within each unit cell of two MOFs (Figs. 3(b) and 3(e)). This indicates the formation of  $C_2H_2$  clusters due to the radial-like  $\pi\cdots\pi$  interactions and  $C-H^{\delta+}\cdots C^{\delta-}$  dipole-dipole interactions between  $C_2H_2$  molecules, which were not unveiled in previous work [42]. Thus, each  $C_2H_2$  molecule is stabilized by multiple host-guest and guest-guest interactions in a perfectly cooperative manner within the O- and N-rich channels of MIL-160 and MOF-303, affording their ultrahigh  $C_2H_2$  uptake capacities.

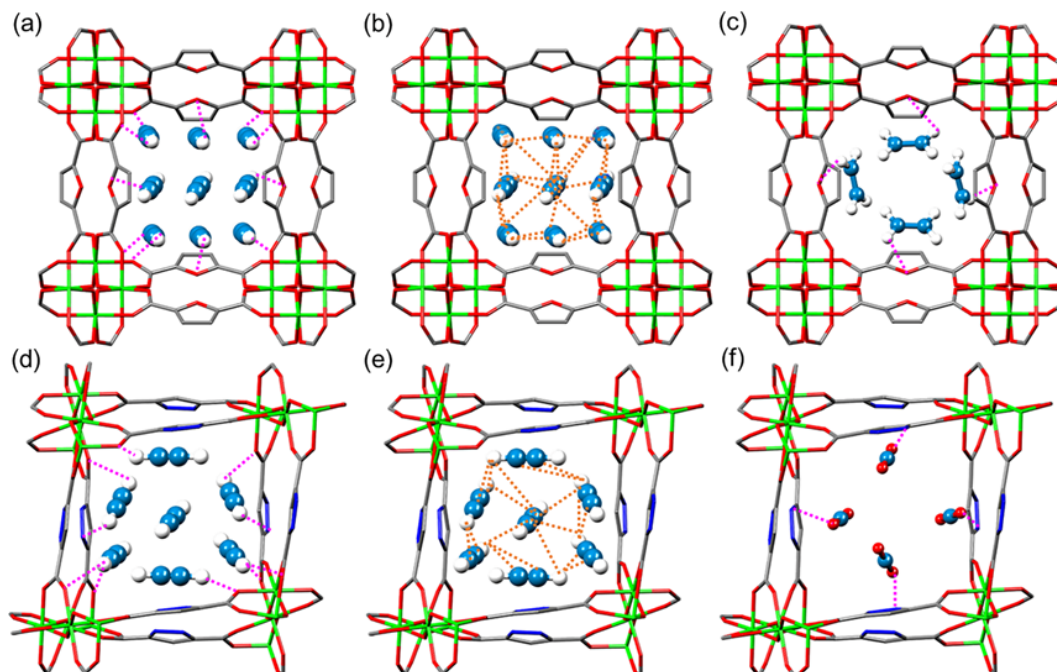


**Figure 3** The commensurate stacking of  $C_2H_2$  molecules in (a) MIL-160 and (d) MOF-303 via host-guest interactions. The visualization of guest-guest interactions between  $C_2H_2$  molecules in (b) MIL-160 and (e) MOF-303. (c)  $C_2H_4$  binding configurations in MIL-160. (f)  $CO_2$  binding configurations in MOF-303. Host-guest interactions are shown in pink dotted lines and intermolecular interactions are shown in orange dotted lines. Color code: Al (green), C (grey), O (red), N (blue), and H (white).

In comparison, the two MOFs can only accommodate with four molecules of  $\text{CO}_2$  and  $\text{C}_2\text{H}_4$  per cell (Figs. 3(c) and 3(f) and Fig. S23 in the ESM), which is attributed to the weaker and less synergistic host-guest (guest-guest) interactions. Additionally, the corresponding binding energies of  $\text{C}_2\text{H}_2$  were calculated to be 35.8 and 33.1  $\text{kJ}\cdot\text{mol}^{-1}$  for MIL-160 and MOF-303, respectively, higher than those of  $\text{CO}_2$  (28.9 and 30.2  $\text{kJ}\cdot\text{mol}^{-1}$ ) and  $\text{C}_2\text{H}_4$  (29.3 and 31.5  $\text{kJ}\cdot\text{mol}^{-1}$ ). The above theoretical observations coherently support the separation potential of these two MOFs for simultaneous separation of  $\text{C}_2\text{H}_2/\text{CO}_2$  and  $\text{C}_2\text{H}_2/\text{C}_2\text{H}_4$  mixtures.

To illustrate the separation performances of two materials, transient breakthrough simulations were firstly conducted for equimolar 50/50  $\text{C}_2\text{H}_2/\text{CO}_2$  and  $\text{C}_2\text{H}_2/\text{C}_2\text{H}_4$  mixtures under ambient conditions (Figs. 4(a) and 4(b)) [46, 47]. The results presented that the clear separation for two mixtures can be achieved with high efficiency. The calculated  $\text{C}_2\text{H}_2$  capture amount on MIL-160 can reach up to 7.3  $\text{mol}\cdot\text{kg}^{-1}$  from two mixtures, consistent with the simulated  $\text{C}_2\text{H}_2$  recovery amount with high purity (Fig. 4(c) and Fig. S24 in the ESM). Such a record high  $\text{C}_2\text{H}_2$  capture amount promoted us to evaluate the actual separation performances. Equally astonishing, excellent separation performances and agreement between the experimental and simulated breakthrough curves were achieved (Figs. S25 and S26 in the ESM). The retention time of  $\text{C}_2\text{H}_2$  in MIL-160 packed column was 161  $\text{min}\cdot\text{g}^{-1}$ , which is not only 2.4 times longer than that of  $\text{CO}_2$  (68  $\text{min}\cdot\text{g}^{-1}$ ) but also an unprecedented value up to now (Fig. 4(d)). Similarly, MOF-303 showed relatively more rapid breakthrough of  $\text{CO}_2$  with selective retention of  $\text{C}_2\text{H}_2$  (retention time of 38 and 87  $\text{min}\cdot\text{g}^{-1}$ , respectively, Fig. 4(e)). The separation factors were calculated to be 10.1 and 2.1, respectively, on MIL-160 and MOF-303 for  $\text{C}_2\text{H}_2/\text{CO}_2$  separation. It is worth noting that the trapping amounts of  $\text{C}_2\text{H}_2$  from the dynamic adsorption of  $\text{C}_2\text{H}_2/\text{CO}_2$  mixtures on MIL-160 and MOF-303 are 201 and 173  $\text{L}\cdot\text{kg}^{-1}$ , 86% and 88% of the saturated uptakes from the single-component isotherms at 298 K and 1.0 bar. Remarkably, MIL-160 showed both the highest breakthrough time and  $\text{C}_2\text{H}_2$  capture amount among all of the top-performing materials under the same mixed gas flow rate of 2  $\text{mL}\cdot\text{min}^{-1}$  at 298 K, i.e., ATC-Cu

(132  $\text{min}\cdot\text{g}^{-1}$  and 103  $\text{L}\cdot\text{kg}^{-1}$ ) [48], FJI-H8-Me (89  $\text{min}\cdot\text{g}^{-1}$  and 194  $\text{L}\cdot\text{kg}^{-1}$ ) [49], and SNNU-45 (79  $\text{min}\cdot\text{g}^{-1}$  and 115  $\text{L}\cdot\text{kg}^{-1}$ ) [29] (Fig. 4(f) and Fig. S26 in the ESM).

For  $\text{C}_2\text{H}_2/\text{C}_2\text{H}_4$  separation, the eluted time for  $\text{C}_2\text{H}_2$ : 157 and 92  $\text{min}\cdot\text{g}^{-1}$  in MIL-160 and MOF-303, respectively, was much longer than that of  $\text{C}_2\text{H}_4$ : 71 and 42  $\text{min}\cdot\text{g}^{-1}$  in MIL-160 and MOF-303, respectively. These observations indicate that the ultrahigh  $\text{C}_2\text{H}_2$  uptakes and good selectivity of MIL-160 and MOF-303 were well maintained under mixed-gas dynamic conditions. The two MOFs also showed a significantly higher elution time of  $\text{C}_2\text{H}_2$  than that of CAU-10-H (Fig. S28 in the ESM), which further confirmed the superior  $\text{C}_2\text{H}_2$  adsorption performance of the two MOFs. Notably, among all candidates, MIL-160 has the greatest potential in overcoming the problem of the trade-off between  $\text{C}_2\text{H}_2$  uptake and selectivity. And the cyclic breakthrough tests revealed that MIL-160 retained the excellent  $\text{C}_2\text{H}_2$  capture performance after six cycles, validating the good recyclability of MIL-160 for  $\text{C}_2\text{H}_2/\text{C}_2\text{H}_4$  and  $\text{C}_2\text{H}_2/\text{CO}_2$  separations (Fig. S29 in the ESM). Taken together, these results demonstrate that the challenging  $\text{C}_2\text{H}_2/\text{C}_2\text{H}_4$  and  $\text{C}_2\text{H}_2/\text{CO}_2$  separations can be satisfactorily addressed using MIL-160 and MOF-303 under ambient conditions.

### 3 Conclusions

To summarize, the combination of pore confinement and commensurate stacking effects was employed as a powerful strategy to efficiently trap  $\text{C}_2\text{H}_2$  from both  $\text{CO}_2$  and  $\text{C}_2\text{H}_4$ . Owing to the suitable 1D channels lined by periodically interspersed molecular recognition sites, MIL-160 and MOF-303 exhibit high  $\text{C}_2\text{H}_2$  affinity, especially MIL-160 registered the highest  $\text{C}_2\text{H}_2$  capacity of 235  $\text{cm}^3\cdot\text{g}^{-1}$  among the reported  $\text{C}_2\text{H}_2$  selective physisorbents (including OMS types). Conversely, only moderate amounts of  $\text{CO}_2$  and  $\text{C}_2\text{H}_4$  were adsorbed onto the model adsorbents, thus giving both high  $\text{C}_2\text{H}_2/\text{CO}_2$  and  $\text{C}_2\text{H}_2/\text{C}_2\text{H}_4$  selectivity. Computational simulations confirmed that the currently occurred commensurate stacking of  $\text{C}_2\text{H}_2$  in the confirmed ultramicropores through multiple host-guest and

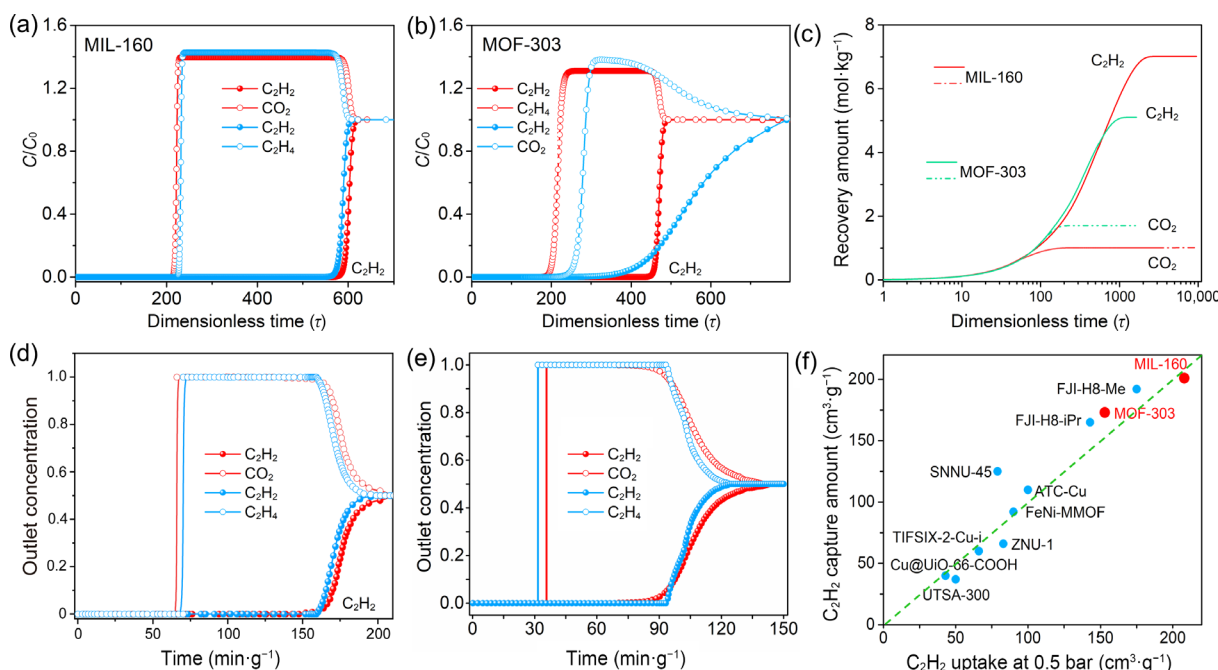


**Figure 4** Simulated breakthrough curves of equimolar  $\text{C}_2\text{H}_2/\text{CO}_2$  and  $\text{C}_2\text{H}_2/\text{C}_2\text{H}_4$  mixtures in (a) MIL-160 and (b) MOF-303 at 298 K and 1.0 bar. (c) Cumulative recovery of  $\text{C}_2\text{H}_2$  and  $\text{CO}_2$  during simulated counter-current blowdown operations. Experimental breakthrough curves of equimolar  $\text{C}_2\text{H}_2/\text{CO}_2$  and  $\text{C}_2\text{H}_2/\text{C}_2\text{H}_4$  mixtures on (d) MIL-160 and (e) MOF-303 at 298 K and 1.0 bar. (f) The comparison of adsorption and separation performances for equimolar  $\text{C}_2\text{H}_2/\text{CO}_2$  mixture on various MOFs with the same gas flow rate of 2  $\text{mL}\cdot\text{min}^{-1}$  at 298 K.

guest–guest interactions would account for the ultrahigh C<sub>2</sub>H<sub>2</sub> storage capacity. Through this commensurate stacking strategy, the ability of the model MOFs to fruitfully couple record-high C<sub>2</sub>H<sub>2</sub> uptake and outstanding selectivity over CO<sub>2</sub> and C<sub>2</sub>H<sub>4</sub> was highlighted. This work would not only provide insights into the strategy of the cogeneration of gas cluster and commensurate stacking through maximization of host–guest and guest–guest interactions within the confined pores containing arrayed binding sites, but also pave new avenues for pore engineering in gas adsorption and separation.

## Acknowledgements

This work was supported by the National Natural Science Foundation of China (No. 21868002) and Dean Project of Guangxi Key Laboratory of Petrochemical Resource Processing and Process Intensification Technology (No. 2021Z010).

**Electronic Supplementary Material:** Supplementary material (details of the experimental section, PXRD patterns, BET surface area, single-component adsorption isotherms measure at different temperature, the results of calculated  $Q_{st}$  and IAST selectivity, the fitting parameters of the virial equation, the fitting parameters of adsorption isotherms based on dual-site Langmuir–Freundlich (DSLFF) models, the cyclic breakthrough curves, the results of molecular simulations, the simulated breakthrough experimental results, cumulative purity of C<sub>2</sub>H<sub>2</sub> recovered from MIL-160 and MOF-303 during simulated counter-current blowdown operations, and the comparison of adsorption capacity and selectivity with virous materials) is available in the online version of this article at <https://doi.org/10.1007/s12274-022-5346-7>.

**Open Access** This article is licensed under a Creative Commons Attribution 4.0 International License, which permits use, sharing, adaptation, distribution and reproduction in any medium or format, as long as you give appropriate credit to the original author(s) and the source, provide a link to the Creative Commons licence, and indicate if changes were made.

The images or other third party material in this article are included in the article's Creative Commons licence, unless indicated otherwise in a credit line to the material. If material is not included in the article's Creative Commons licence and your intended use is not permitted by statutory regulation or exceeds the permitted use, you will need to obtain permission directly from the copyright holder.

To view a copy of this licence, visit <http://creativecommons.org/licenses/by/4.0/>.

## References

- Lin, R. B.; Li, L. B.; Wu, H.; Arman, H.; Li, B.; Lin, R. G.; Zhou, W.; Chen, B. L. Optimized separation of acetylene from carbon dioxide and ethylene in a microporous material. *J. Am. Chem. Soc.* **2017**, *139*, 8022–8028.
- Chen, K. J.; Scott, H. S.; Madden, D. G.; Pham, T.; Kumar, A.; Bajpai, A.; Lusi, M.; Forrest, K. A.; Space, B.; Perry IV, J. J. et al. Benchmark C<sub>2</sub>H<sub>2</sub>/CO<sub>2</sub> and CO<sub>2</sub>/C<sub>2</sub>H<sub>2</sub> separation by two closely related hybrid ultramicroporous materials. *Chem* **2016**, *1*, 753–765.
- Shen, J.; He, X.; Ke, T.; Krishna, R.; van Baten, J. M.; Chen, R. D.; Bao, Z. B.; Xing, H. B.; Dincă, M.; Zhang, Z. G. et al. Simultaneous interlayer and intralayer space control in two-dimensional metal-organic frameworks for acetylene/ethylene separation. *Nat. Commun.* **2020**, *11*, 6259.
- Liu, S. S.; Han, X.; Chai, Y. C.; Wu, G. J.; Li, W. Y.; Li, J. N.; da Silva, I.; Manuel, P.; Cheng, Y. Q.; Daemen, L. L. et al. Efficient separation of acetylene and carbon dioxide in a decorated zeolite. *Angew. Chem., Int. Ed.* **2021**, *60*, 6526–6532.
- Schobert, H. Production of acetylene and acetylene-based chemicals from coal. *Chem. Rev.* **2014**, *114*, 1743–1760.
- Mukherjee, S.; Kumar, N.; Bezrukov, A. A.; Tan, K.; Pham, T.; Forrest, K. A.; Oyekan, K. A.; Qazvini, O. T.; Madden, D. G.; Space, B. et al. Amino-functionalised hybrid ultramicroporous materials that enable single-step ethylene purification from a ternary mixture. *Angew. Chem., Int. Ed.* **2021**, *60*, 10902–10909.
- Zhang, Y. B.; Yang, L. F.; Wang, L. Y.; Duttwyler, S.; Xing, H. B. A microporous metal-organic framework supramolecularly assembled from a Cu(II) dodecaborate cluster complex for selective gas separation. *Angew. Chem.* **2019**, *131*, 8229–8234.
- Luna-Triguero, A.; Vicent-Luna, J. M.; Madero-Castro, R. M.; Gómez-Álvarez, P.; Calero, S. Acetylene storage and separation using metal-organic frameworks with open metal sites. *ACS Appl. Mater. Interfaces* **2019**, *11*, 31499–31507.
- Qazvini, O. T.; Babarao, R.; Telfer, S. G. Multipurpose metal-organic framework for the adsorption of acetylene: Ethylene purification and carbon dioxide removal. *Chem. Mater.* **2019**, *31*, 4919–4926.
- Qazvini, O. T.; Macreadie, L. K.; Telfer, S. G. Effect of ligand functionalization on the separation of small hydrocarbons and CO<sub>2</sub> by a series of MUF-15 analogues. *Chem. Mater.* **2020**, *32*, 6744–6752.
- Xu, T. T.; Jiang, Z. Z.; Liu, P. X.; Chen, H. N.; Lan, X. S.; Chen, D. L.; Li, L. B.; He, Y. B. Immobilization of oxygen atoms in the pores of microporous metal-organic frameworks for C<sub>2</sub>H<sub>2</sub> separation and purification. *ACS Appl. Nano Mater.* **2020**, *3*, 2911–2919.
- Qian, Q. L.; Gu, X. W.; Pei, J. Y.; Wen, H. M.; Wu, H.; Zhou, W.; Li, B.; Qian, G. D. A novel anion-pillared metal-organic framework for highly efficient separation of acetylene from ethylene and carbon dioxide. *J. Mater. Chem. A* **2021**, *9*, 9248–9255.
- Zhang, Y. B.; Hu, J. B.; Krishna, R.; Wang, L. Y.; Yang, L. F.; Cui, X. L.; Duttwyler, S.; Xing, H. B. Rational design of microporous MOFs with anionic boron cluster functionality and cooperative dihydrogen binding sites for highly selective capture of acetylene. *Angew. Chem.* **2020**, *132*, 17817–17822.
- Peng, Y. L.; Pham, T.; Li, P. F.; Wang, T.; Chen, Y.; Chen, K. J.; Forrest, K. A.; Space, B.; Cheng, P.; Zaworotko, M. J. et al. Robust ultramicroporous metal-organic frameworks with benchmark affinity for acetylene. *Angew. Chem., Int. Ed.* **2018**, *57*, 10971–10975.
- Dutta, S.; Mukherjee, S.; Qazvini, O. T.; Gupta, A. K.; Sharma, S.; Mahato, D.; Babarao, R.; Ghosh, S. K. Three-in-one C<sub>2</sub>H<sub>2</sub>-selectivity-guided adsorptive separation across an isorecticular family of cationic square-lattice MOFs. *Angew. Chem., Int. Ed.* **2022**, *61*, e202114132.
- Zhai, Q. G.; Bu, X. H.; Mao, C. Y.; Zhao, X.; Daemen, L.; Cheng, Y. Q.; Ramirez-Cuesta, A. J.; Feng, P. Y. An ultra-tunable platform for molecular engineering of high-performance crystalline porous materials. *Nat. Commun.* **2016**, *7*, 13645.
- Xiang, S. C.; Zhou, W.; Gallegos, J. M.; Liu, Y.; Chen, B. L. Exceptionally high acetylene uptake in a microporous metal-organic framework with open metal sites. *J. Am. Chem. Soc.* **2009**, *131*, 12415–12419.
- Pang, J. D.; Jiang, F. L.; Wu, M. Y.; Liu, C. P.; Su, K. Z.; Lu, W. G.; Yuan, D. Q.; Hong, M. C. A porous metal-organic framework with ultrahigh acetylene uptake capacity under ambient conditions. *Nat. Commun.* **2015**, *6*, 7575.
- Luo, F.; Yan, C. S.; Dang, L. L.; Krishna, R.; Zhou, W.; Wu, H.; Dong, X. L.; Han, Y.; Hu, T. L.; O'Keeffe, M. et al. UTSA-74: A MOF-74 isomer with two accessible binding sites per metal center for highly selective gas separation. *J. Am. Chem. Soc.* **2016**, *138*, 5678–5684.
- Xiang, S. C.; Zhou, W.; Zhang, Z. J.; Green, M. A.; Liu, Y.; Chen, B. L. Open metal sites within isostructural metal-organic frameworks for differential recognition of acetylene and extraordinarily high acetylene storage capacity at room temperature. *Angew. Chem., Int. Ed.* **2010**, *49*, 4615–4618.
- Rao, X. T.; Cai, J. F.; Yu, J. C.; He, Y. B.; Wu, C. D.; Zhou, W.; Yildirim, T.; Chen, B. L.; Qian, G. D. A microporous metal-organic framework with both open metal and Lewis basic pyridyl sites for

- high C<sub>2</sub>H<sub>2</sub> and CH<sub>4</sub> storage at room temperature. *Chem. Commun.* **2013**, *49*, 6719–6721.
- [22] Cui, X. L.; Chen, K. J.; Xing, H. B.; Yang, Q. W.; Krishna, R.; Bao, Z. B.; Wu, H.; Zhou, W.; Dong, X. L.; Han, Y. et al. Pore chemistry and size control in hybrid porous materials for acetylene capture from ethylene. *Science* **2016**, *353*, 141–144.
- [23] Zhang, Z. Q.; Cui, X. L.; Yang, L. F.; Cui, J. Y.; Bao, Z. B.; Yang, Q. W.; Xing, H. B. Hexafluorogermanate (GeFSIX) anion-functionalized hybrid ultramicroporous materials for efficiently trapping acetylene from ethylene. *Ind. Eng. Chem. Res.* **2018**, *57*, 7266–7274.
- [24] Li, Q.; Wu, N. N.; Li, J.; Wu, D. P. A highly connected trinuclear cluster based metal-organic framework for efficient separation of C<sub>2</sub>H<sub>2</sub>/C<sub>2</sub>H<sub>4</sub> and C<sub>2</sub>H<sub>2</sub>/CO<sub>2</sub>. *Inorg. Chem.* **2020**, *59*, 13005–13008.
- [25] Zhang, Z. Q.; Peh, S. B.; Wang, Y. X.; Kang, C. J.; Fan, W. D.; Zhao, D. Efficient trapping of trace acetylene from ethylene in an ultramicroporous metal-organic framework: Synergistic effect of high-density open metal and electronegative sites. *Angew. Chem.* **2020**, *132*, 19089–19094.
- [26] Zhang, J. W.; Hu, M. C.; Li, S. N.; Jiang, Y. C.; Qu, P.; Zhai, Q. G. Assembly of [Cu<sub>2</sub>(COO)<sub>4</sub>] and [M<sub>3</sub>(μ<sub>3</sub>-O)(COO)<sub>6</sub>] (M = Sc, Fe, Ga, and In) building blocks into porous frameworks towards ultra-high C<sub>2</sub>H<sub>2</sub>/CO<sub>2</sub> and C<sub>2</sub>H<sub>2</sub>/CH<sub>4</sub> separation performance. *Chem. Commun.* **2018**, *54*, 2012–2015.
- [27] Foo, M. L.; Matsuda, R.; Hijikata, Y.; Krishna, R.; Sato, H.; Horike, S.; Hori, A.; Duan, J. G.; Sato, Y.; Kubota, Y. et al. An adsorbate discriminatory gate effect in a flexible porous coordination polymer for selective adsorption of CO<sub>2</sub> over C<sub>2</sub>H<sub>2</sub>. *J. Am. Chem. Soc.* **2016**, *138*, 3022–3030.
- [28] Jiang, X.; Pham, T.; Cao, J. W.; Forrest, K. A.; Wang, H.; Chen, J.; Zhang, Q. Y.; Chen, K. J. Molecular sieving of acetylene from ethylene in a rigid ultra-microporous metal organic framework. *Chem.—Eur. J.* **2021**, *27*, 9446–9453.
- [29] Li, Y. P.; Wang, Y.; Xue, Y. Y.; Li, H. P.; Zhai, Q. G.; Li, S. N.; Jiang, Y. C.; Hu, M. C.; Bu, X. H. Ultramicroporous building units as a path to Bi-microporous metal-organic frameworks with high acetylene storage and separation performance. *Angew. Chem.* **2019**, *131*, 13724–13729.
- [30] Lee, J.; Chuah, C. Y.; Kim, J.; Kim, Y.; Ko, N.; Seo, Y.; Kim, K.; Bae, T. H.; Lee, E. Separation of acetylene from carbon dioxide and ethylene by a water-stable microporous metal-organic framework with aligned imidazolium groups inside the channels. *Angew. Chem.* **2018**, *130*, 7995–7999.
- [31] Kumar, N.; Mukherjee, S.; Harvey-Reid, N. C.; Bezrukov, A. A.; Tan, K.; Martins, V.; Vandichel, M.; Pham, T.; van Wyk, L. M.; Oyekan, K. et al. Breaking the trade-off between selectivity and adsorption capacity for gas separation. *Chem* **2021**, *7*, 3085–3098.
- [32] Fan, W. D.; Yuan, S.; Wang, W. J.; Feng, L.; Liu, X. P.; Zhang, X. R.; Wang, X.; Kang, Z. X.; Dai, F. N.; Yuan, D. Q. et al. Optimizing multivariate metal-organic frameworks for efficient C<sub>2</sub>H<sub>2</sub>/CO<sub>2</sub> separation. *J. Am. Chem. Soc.* **2020**, *142*, 8728–8737.
- [33] Fan, L. H.; Yue, L. L.; Sun, W. Q.; Wang, X. X.; Zhou, P.; Zhang, Y. B.; He, Y. B. Ligand bent-angle engineering for tuning topological structures and acetylene purification performances of copper-diisophthalate frameworks. *ACS Appl. Mater. Interfaces* **2021**, *13*, 40788–40797.
- [34] Li, B.; Cui, X. L.; O’Nolan, D.; Wen, H. M.; Jiang, M. D.; Krishna, R.; Wu, H.; Lin, R. B.; Chen, Y. S.; Yuan, D. Q. et al. An ideal molecular sieve for acetylene removal from ethylene with record selectivity and productivity. *Adv. Mater.* **2017**, *29*, 1704210.
- [35] Hu, T. L.; Wang, H. L.; Li, B.; Krishna, R.; Wu, H.; Zhou, W.; Zhao, Y. F.; Han, Y.; Wang, X.; Zhu, W. D. et al. Microporous metal-organic framework with dual functionalities for highly efficient removal of acetylene from ethylene/acetylene mixtures. *Nat. Commun.* **2015**, *6*, 7328.
- [36] Li, H.; Liu, C. P.; Chen, C.; Di, Z. Y.; Yuan, D. Q.; Pang, J. D.; Wei, W.; Wu, M. Y.; Hong, M. C. An unprecedented pillar-cage fluorinated hybrid porous framework with highly efficient acetylene storage and separation. *Angew. Chem.* **2021**, *133*, 7625–7630.
- [37] Yao, Z. Z.; Zhang, Z. J.; Liu, L. Z.; Li, Z. Y.; Zhou, W.; Zhao, Y. F.; Han, Y.; Chen, B. L.; Krishna, R.; Xiang, S. C. Extraordinary separation of acetylene-containing mixtures with microporous metal-organic frameworks with open O donor sites and tunable robustness through control of the helical chain secondary building units. *Chem.—Eur. J.* **2016**, *22*, 5676–5683.
- [38] Xue, Y. Y.; Bai, X. Y.; Zhang, J.; Wang, Y.; Li, S. N.; Jiang, Y. C.; Hu, M. C.; Zhai, Q. G. Precise pore space partitions combined with high-density hydrogen-bonding acceptors within metal-organic frameworks for highly efficient acetylene storage and separation. *Angew. Chem., Int. Ed.* **2021**, *60*, 10122–10128.
- [39] Ye, Y. X.; Ma, Z. L.; Lin, R. B.; Krishna, R.; Zhou, W.; Lin, Q. J.; Zhang, Z. J.; Xiang, S. C.; Chen, B. L. Pore space partition within a metal-organic framework for highly efficient C<sub>2</sub>H<sub>2</sub>/CO<sub>2</sub> separation. *J. Am. Chem. Soc.* **2019**, *141*, 4130–4136.
- [40] Pei, J. Y.; Wen, H. M.; Gu, X. W.; Qian, Q. L.; Yang, Y.; Cui, Y. J.; Li, B.; Chen, B. L.; Qian, G. D. Dense packing of acetylene in a stable and low-cost metal-organic framework for efficient C<sub>2</sub>H<sub>2</sub>/CO<sub>2</sub> separation. *Angew. Chem.* **2021**, *133*, 25272–25278.
- [41] Zhang, X.; Lin, R. B.; Wu, H.; Huang, Y. H.; Ye, Y. X.; Duan, J. G.; Zhou, W.; Li, J. R.; Chen, B. L. Maximizing acetylene packing density for highly efficient C<sub>2</sub>H<sub>2</sub>/CO<sub>2</sub> separation through immobilization of amine sites within a prototype MOF. *Chem. Eng. J.* **2022**, *431*, 134184.
- [42] Ye, Y. X.; Xian, S. K.; Cui, H.; Tan, K.; Gong, L. S.; Liang, B.; Pham, T.; Pandey, H.; Krishna, R.; Lan, P. C. et al. Metal-organic framework based hydrogen-bonding nanotrap for efficient acetylene storage and separation. *J. Am. Chem. Soc.* **2022**, *144*, 1681–1689.
- [43] Bao, Z. B.; Wang, J. W.; Zhang, Z. G.; Xing, H. B.; Yang, Q. W.; Yang, Y. W.; Wu, H.; Krishna, R.; Zhou, W.; Chen, B. L. et al. Molecular sieving of ethane from ethylene through the molecular cross-section size differentiation in gallate-based metal-organic frameworks. *Angew. Chem.* **2018**, *130*, 16252–16257.
- [44] Wang, L. Y.; Sun, W. Q.; Zhang, Y. B.; Xu, N.; Krishna, R.; Hu, J. B.; Jiang, Y. J.; He, Y. B.; Xing, H. B. Interpenetration symmetry control within ultramicroporous robust boron cluster hybrid MOFs for benchmark purification of acetylene from carbon dioxide. *Angew. Chem., Int. Ed.* **2021**, *60*, 22865–22870.
- [45] Gong, W.; Cui, H.; Xie, Y.; Li, Y. G.; Tang, X. H.; Liu, Y.; Cui, Y.; Chen, B. L. Efficient C<sub>2</sub>H<sub>2</sub>/CO<sub>2</sub> separation in ultramicroporous metal-organic frameworks with record C<sub>2</sub>H<sub>2</sub> storage density. *J. Am. Chem. Soc.* **2021**, *143*, 14869–14876.
- [46] Krishna, R. Methodologies for screening and selection of crystalline microporous materials in mixture separations. *Sep. Purif. Technol.* **2018**, *194*, 281–300.
- [47] Krishna, R. Metrics for evaluation and screening of metal-organic frameworks for applications in mixture separations. *ACS Omega* **2020**, *5*, 16987–17004.
- [48] Niu, Z.; Cui, X. L.; Pham, T.; Verma, G.; Lan, P. C.; Shan, C.; Xing, H. B.; Forrest, K. A.; Suepaul, S.; Space, B. et al. A MOF-based ultra-strong acetylene nano-trap for highly efficient C<sub>2</sub>H<sub>2</sub>/CO<sub>2</sub> separation. *Angew. Chem.* **2021**, *133*, 5343–5348.
- [49] Di, Z. Y.; Liu, C. P.; Pang, J. D.; Chen, C.; Hu, F. L.; Yuan, D. Q.; Wu, M. Y.; Hong, M. C. Cage-like porous materials with simultaneous high C<sub>2</sub>H<sub>2</sub> storage and excellent C<sub>2</sub>H<sub>2</sub>/CO<sub>2</sub> separation performance. *Angew. Chem., Int. Ed.* **2021**, *60*, 10828–10832.

# Electronic Supplementary Material

## Commensurate stacking within confined ultramicropores boosting acetylene storage capacity and separation efficiency

Zhengkui Huang<sup>1</sup>, Kungang Chai<sup>1</sup>, Chengjun Kang<sup>2</sup>, Rajamani Krishna<sup>3</sup> (✉), and Zhaoqiang Zhang<sup>2</sup> (✉)

<sup>1</sup> Guangxi Key Laboratory of Petrochemical Resource Processing and Process Intensification Technology, School of Chemistry and Chemical Engineering, Guangxi University, Nanning 530004, China

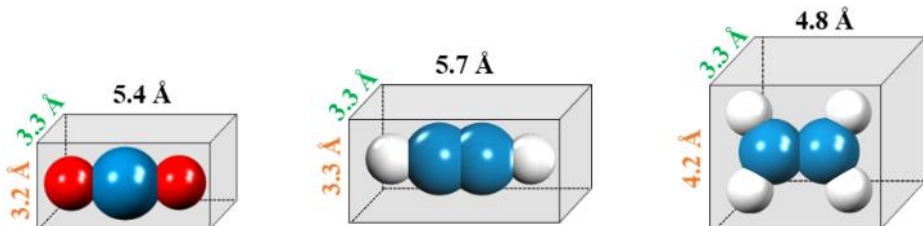
<sup>2</sup> Department of Chemical and Biomolecular Engineering, National University of Singapore, Singapore 117585, Singapore

<sup>3</sup> Van't Hoff Institute for Molecular Sciences, University of Amsterdam, Park 904, Amsterdam 1098 XH, The Netherlands

Supporting information to <https://doi.org/10.1007/s12274-022-5346-7>

### S1 Physical and structural properties of gas molecules

**Table S1** Physical and structural properties of CO<sub>2</sub>, C<sub>2</sub>H<sub>2</sub> and C<sub>2</sub>H<sub>4</sub> molecules [1, 2]



Gas molecule	Carbon dioxide (CO <sub>2</sub> )	Acetylene (C <sub>2</sub> H <sub>2</sub> )	Ethylene (C <sub>2</sub> H <sub>4</sub> )
Dimensions (Å <sup>3</sup> )	5.4×3.3×3.2	5.7×3.3×3.3	4.8×3.3×4.2
Kinetic Diameter (Å)	3.3	3.3	4.2
Polarizability (Å <sup>3</sup> )	2.9	3.3	4.3
Boiling point (K)	194.7	189.3	169.3
Dipole moment (×10 <sup>18</sup> esu cm)	0	0	0
Quadrupole moment (×10 <sup>-26</sup> esu cm <sup>2</sup> )	4.3	7.2	1.5



## S2. Experimental section and gas isotherms

### 2.1. Materials

All chemicals and solvents were commercially available and used directly without further purification: aluminum chloride hexahydrate ( $\text{AlCl}_3 \cdot 6\text{H}_2\text{O}$ , 97%), sodium hydroxide (NaOH, 99.5%), methanol (MeOH, 99%) were purchased from Aladdin, Shanghai, China. 2,5-Furandicarboxylic acid (FDC, 98%), 3,5-pyrazoledicarboxylic acid monohydrate ( $\text{H}_2\text{PZDC}$ , 99%) were purchased from Macklin, Shanghai, China.

### 2.2 Preparation of MIL-160 and MOF-303

MIL-160 was prepared via a microwave synthesis method. Briefly, NaOH (0.08 g, 2 mmol), FDC (0.15 g, 1 mmol), and  $\text{AlCl}_3 \cdot 6\text{H}_2\text{O}$  (0.12 g, 1 mmol) were transferred into a 30 mL glass vial, then with 15 mL  $\text{H}_2\text{O}$  added. The sealed vial was treated via ultrasonic water bath for 5 min, then heated in the microwave oven to 120 °C and heated for 30 min whilst stirring with 600 rpm. The product was washed with MeOH and dried in vacuum oven at 333 K. The yield was 0.137 g (cal. 90.1% relative to the mass of FDC).

MOF-303 was synthesized using the similar way. Briefly, to a mixture of NaOH (0.08 g, 2 mmol),  $\text{H}_2\text{PZDC}$  (0.38 g, 2.1 mmol) and  $\text{AlCl}_3 \cdot 6\text{H}_2\text{O}$  (0.151 g, 1 mmol) in a 30 mL glass vial, 15 mL  $\text{H}_2\text{O}$  were added carefully. the sealed vial was heated in the microwave oven to 120 °C and kept at this temperature for 30 min while stirring with 600 rpm. After cooling, the solid product was filtered off and washed with MeOH and dried under vacuum at 333 K overnight. The yield was 0.335 g (cal. 88.2% relative to the molar of  $\text{H}_2\text{PZDC}$ ).

The phase purity and crystallinity of the obtained MOFs were characterized by powder X-ray diffraction (PXRD) on a Smartlab-3kw diffractometer (Rigaku) using Cu K $\alpha$  radiation (40 kV and 30 mA) in a scanning range of 5-50 ° at a step speed of 6 ° min<sup>-1</sup>. Before testing, as-synthesized MIL-160 and MOF-303 were solvent-exchanged for several times with methane for 3 days to obtain the guest-free samples. Then the solvent-exchanged samples were vacuum degassed for 12 hours at 373 K. For the stability test, firstly, the samples of MIL-160 and MOF-303 (100 mg per) were immersed into water at ambient conditions for 1, 3, 5, 7 days before characterization.

$\text{N}_2$  adsorption-desorption isotherms at 77 K using liquid nitrogen were measured with a surface area and porosity analyzer (Micromeritics ASAP 2460), which were used to study the porosity of MIL-160 and MOF-303. The Brunauer-Emmett-Teller (BET) surface area ( $S_{\text{BET}}$ ) were calculated according to the Rouquerol consistency criteria (with a linearity of fitting:  $R > 0.99999$ ); total pore volume ( $V_{\text{total}}$ )

was obtained by Gurvich-rule at  $P/P_0=0.95$ . Pore size distributions (PSD) were given on the basis of Horvath-Kawazoe (HK) method. Afterwards, the isotherms of  $C_2H_2$ ,  $CO_2$  and  $C_2H_4$  at 273, 298, and 313 K were measured at pressure ranging from 0-1.0 bar. The test temperatures were controlled by putting the sample tube into a circulating water bath or ice water bath. The mass of samples for isotherms measurement was about 100 mg, and the samples were degassed by dynamic vacuuming process under 393 K for 12 h before each isotherm measurement.

**Table S2** Summary of pore properties for MIL-160 and MOF-303

MOFs	MIL-160	MOF-303
Crystal density ( $g\ cm^{-3}$ )	1.10	1.16
$S_{BET}$ ( $m^2\ g^{-1}$ )	1110	1343
$S_{BET}$ in literatures ( $m^2\ g^{-1}$ )	830 [3]	989 [4]
Pore volume ( $cm^3\ g^{-1}$ )	0.46	0.56
Pore volume in literatures ( $cm^3\ g^{-1}$ )	0.4 [3]	0.54 [4]
Pore size ( $\text{\AA}$ )	4.1	5.9
Pore size in literatures ( $\text{\AA}$ )	4.2 [3]	6 [4]

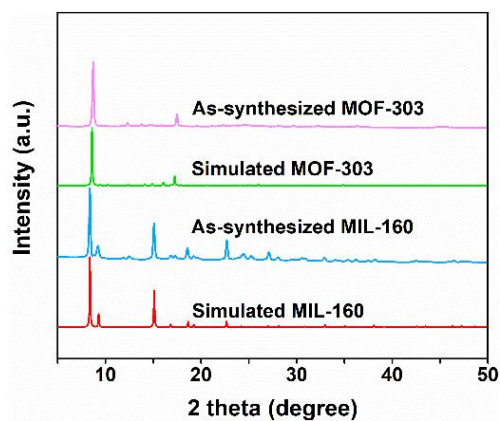


**Figure S1** XRD patterns of MIL-160 and MOF-303.

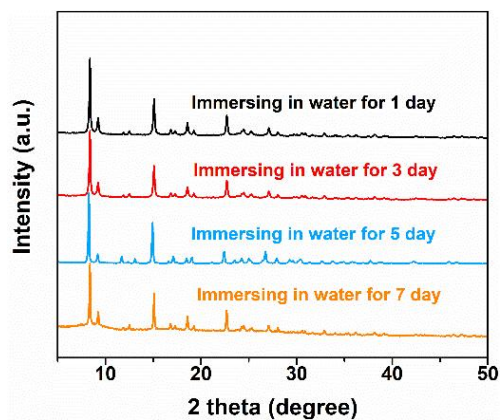


Figure S2 XRD patterns of MIL-160 after immersing in water for different days.

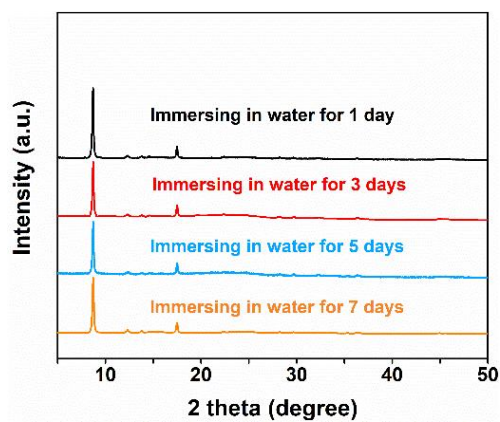


Figure S3 XRD patterns of MOF-303 after immersing in water for different days.

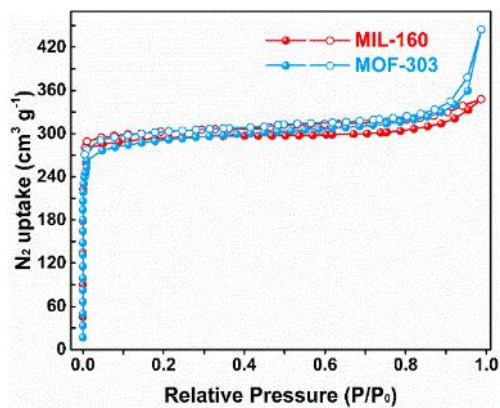


Figure S4  $N_2$  adsorption-desorption isotherms of MIL-160 and MOF-303 at 77 K.

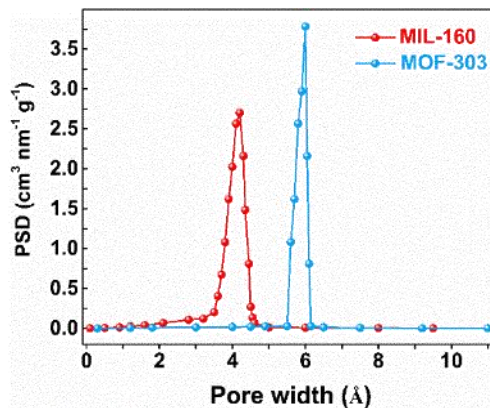


Figure S5 Pore size distribution of MIL-160 and MOF-303.

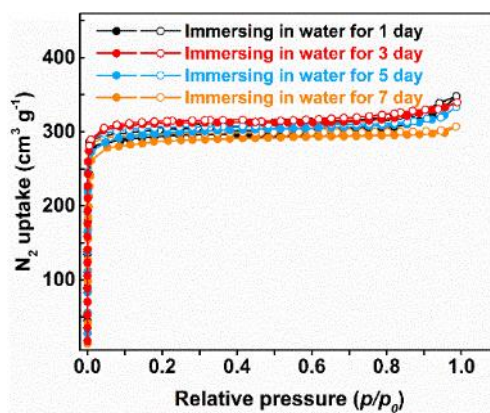


Figure S6 N<sub>2</sub> adsorption-desorption isotherms (77 K) of MIL-160 after immersing in water for different days.

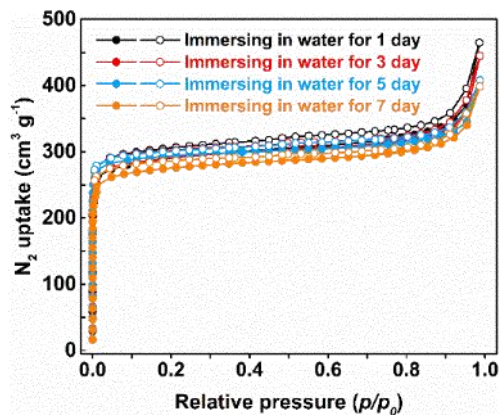


Figure S7 N<sub>2</sub> adsorption-desorption isotherms (77 K) of MOF-303 after immersing in water for different days.

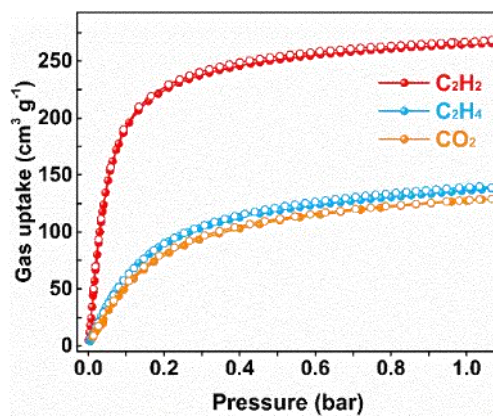


Figure S8 The isotherms of C<sub>2</sub>H<sub>2</sub>, C<sub>2</sub>H<sub>4</sub>, and CO<sub>2</sub> on MIL-160 at 273 K.

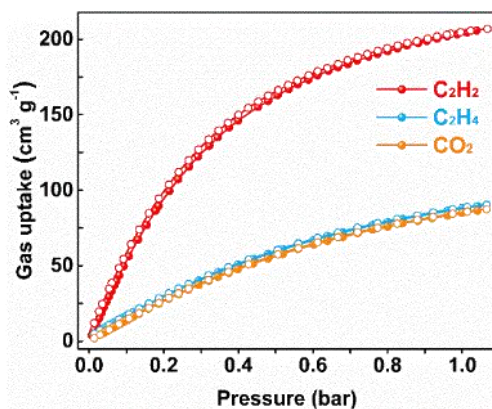


Figure S9 The isotherms of C<sub>2</sub>H<sub>2</sub>, C<sub>2</sub>H<sub>4</sub>, and CO<sub>2</sub> on MIL-160 at 313 K.

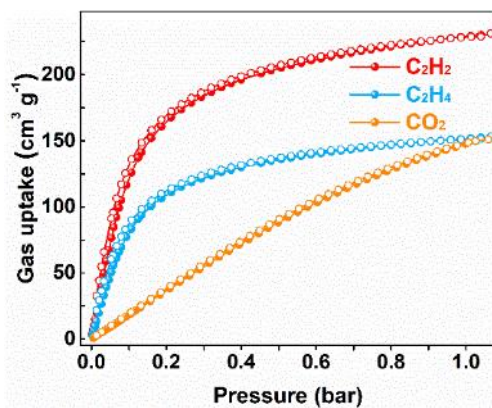


Figure S10 The isotherms of C<sub>2</sub>H<sub>2</sub>, C<sub>2</sub>H<sub>4</sub>, and CO<sub>2</sub> on MOF-303 at 273 K.

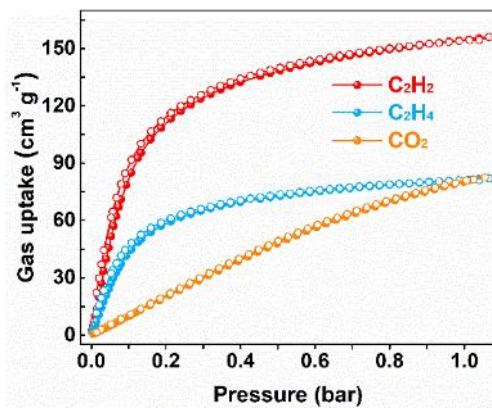
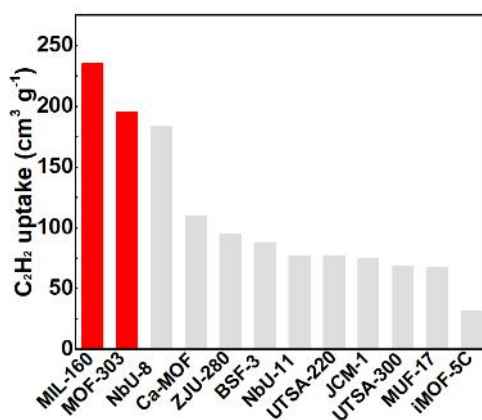


Figure S11 The isotherms of C<sub>2</sub>H<sub>2</sub>, C<sub>2</sub>H<sub>4</sub>, and CO<sub>2</sub> on MOF-303 at 313 K.



**Figure S12** Comparison of C<sub>2</sub>H<sub>2</sub> uptake on the top-performing materials at 298 K and 1.0 bar.

### S3. Selectivity and heat of adsorption calculations.

The unary isotherm data for C<sub>2</sub>H<sub>2</sub>, C<sub>2</sub>H<sub>4</sub>, and CO<sub>2</sub> in the MIL-160, and MOF-303 measured at 298 K were fitted with either the 1-site or 2-site Langmuir model:

$$q = \frac{q_{sat,A} b_A p}{1 + b_A p} + \frac{q_{sat,B} b_B p}{1 + b_B p} \quad (S1)$$

where  $q$  (mmol g<sup>-1</sup>) represents the gas uptake at a certain pressure  $p$  (kPa),  $q_{sat,A}$  and  $q_{sat,B}$  (mmol g<sup>-1</sup>) represent the maximum adsorption amounts on sites 1 and 2, respectively,  $b_A$  and  $b_B$  are the adsorption affinity coefficients of sites 1 and 2, respectively. Based on ideal adsorbed solution theory (IAST), the selectivity of C<sub>2</sub>H<sub>2</sub>/C<sub>2</sub>H<sub>4</sub> and C<sub>2</sub>H<sub>2</sub>/CO<sub>2</sub> mixtures was calculated using the following equation:

$$S_{ads} = \frac{x_1 / x_2}{y_1 / y_2} \quad (S2)$$

where  $S_{ads}$  represents for adsorption selectivity of C<sub>2</sub>H<sub>2</sub>/C<sub>2</sub>H<sub>4</sub> and C<sub>2</sub>H<sub>2</sub>/CO<sub>2</sub>.  $x_1$  and  $x_2$  refer to the adsorbed amount of component 1 and 2,  $y_1$  and  $y_2$  are defined as the molar fractions of the component 1 and 2.

A Virial method was applied for the calculation of isosteric heat of adsorption ( $Q_{st}$ ), which could be expressed as following equations:

$$\ln(p) = \ln(N) + \left(\frac{1}{T}\right) \sum_{i=0}^m a_i \times N^i + \sum_{j=0}^n a_j \times N^j \quad (S3)$$

where  $N$  ( $\text{mmol g}^{-1}$ ) refers to the  $\text{C}_2\text{H}_2$ ,  $\text{CO}_2$  and  $\text{C}_2\text{H}_4$  uptake at pressure  $p$  (kPa) and temperature  $T$  (K),  $a_i$  and  $b_j$  represent the Virial coefficients, to fit the isotherms accurately, the number of coefficients  $m$  and  $n$  is required. The virial parameters obtained from virial equation were used for calculation of  $Q_{st}$  of  $\text{C}_2\text{H}_2$ ,  $\text{CO}_2$  and  $\text{C}_2\text{H}_4$ . The  $Q_{st}$  calculation could be described as the equation:

$$Q_{st} = -R \sum_{i=0}^m a_i \times N^i \quad (\text{S4})$$

$Q_{st}$  is the coverage-dependent isosteric heat of adsorption and  $R$  is the universal gas constant.

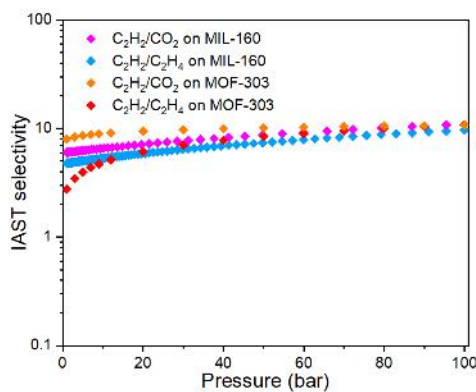


**Figure S13** The selectivity of MIL-160 and MOF-303 for  $\text{C}_2\text{H}_2/\text{CO}_2$  (50/50) and  $\text{C}_2\text{H}_2/\text{C}_2\text{H}_4$  (50/50) mixtures.

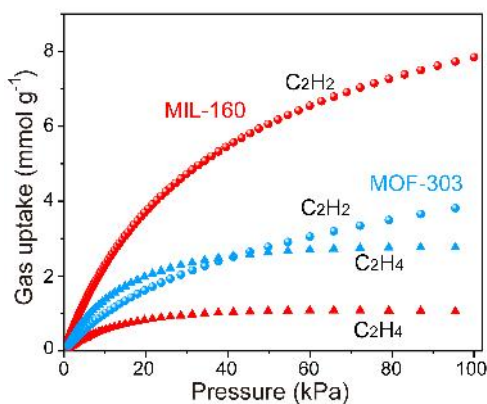


**Figure S14** Predicted mixture adsorption isotherms of MIL-160 and MOF-303 based on IAST for a 50/50  $\text{C}_2\text{H}_2/\text{C}_2\text{H}_4$  mixture at 298 K.



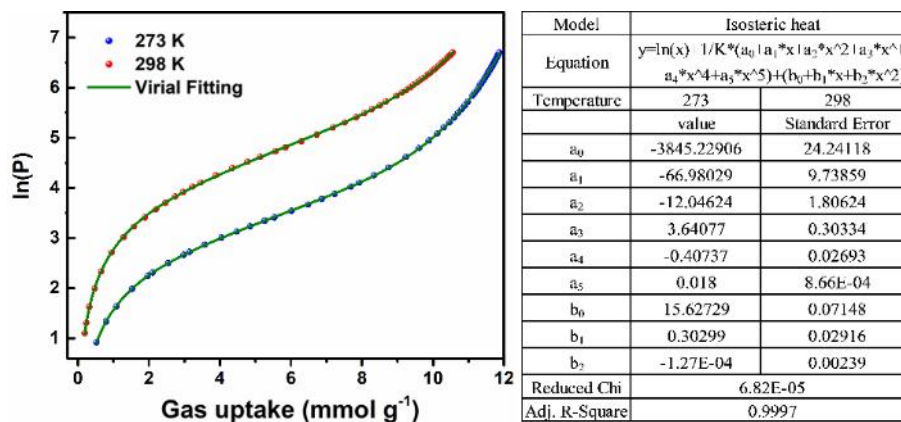


Figure S15  $C_2H_2$  isotherms (points) and Virial fitting curves (lines) of at 298 (red) and 273 K (blue).

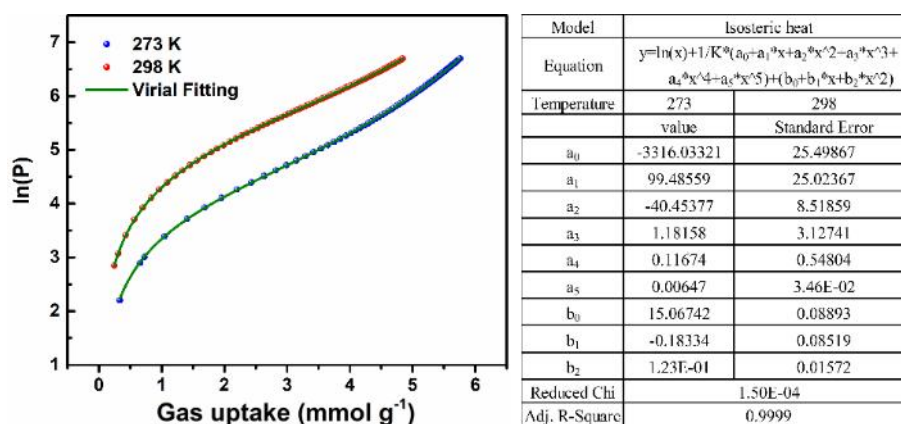


Figure S16  $C_2H_4$  isotherms (points) and Virial fitting curves (lines) of MIL-160 at 298 (red) and 273 K (blue).

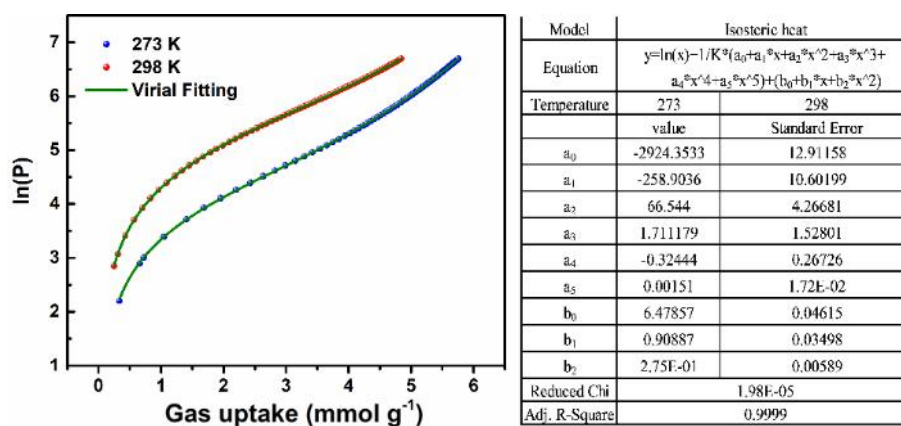
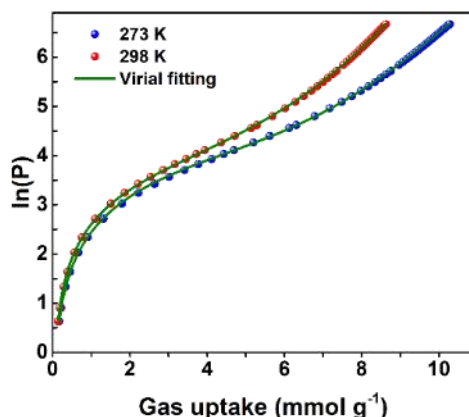
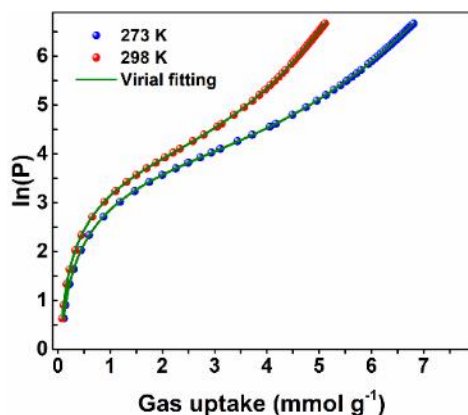


Figure S17  $CO_2$  isotherms (points) and Virial fitting curves (lines) of MIL-160 at 298 (red) and 273 K (blue).



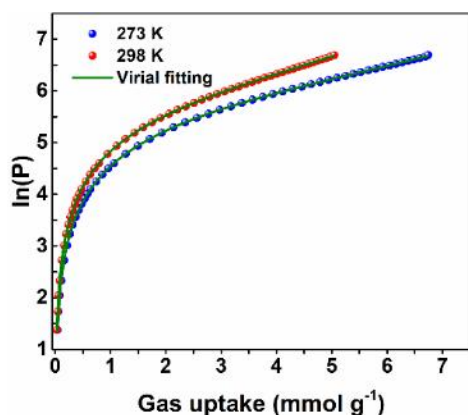
Model		Isosteric heat	
Equation	$y = \ln(x) + 1/K * (a_0 + a_1 * x + a_2 * x^2 + a_3 * x^3 + a_4 * x^4 + a_5 * x^5) + (b_0 - b_1 * x + b_2 * x^2)$		
Temperature	273	298	
	value	Standard Error	
$a_0$	-3523.0067	10.00324	
$a_1$	-58.9036	8.3563	
$a_2$	-13.6668	3.8921	
$a_3$	2.60897	0.8673	
$a_4$	-0.30377	0.26726	
$a_5$	0.00121	2.72E-03	
$b_0$	16.47857	0.05236	
$b_1$	0.80887	0.01498	
$b_2$	1.75E-03	0.00389	
Reduced Chi	5.98E-05		
Adj. R-Square	0.9999		

Figure S18 C<sub>2</sub>H<sub>2</sub> isotherms (points) and Virial fitting curves (lines) of MOF-303 at 298 (red) and 273 K (blue).



Model		Isosteric heat	
Equation	$y = \ln(x) + 1/K * (a_0 + a_1 * x + a_2 * x^2 + a_3 * x^3 + a_4 * x^4 + a_5 * x^5) + (b_0 - b_1 * x + b_2 * x^2)$		
Temperature	273	298	
	value	Standard Error	
$a_0$	-3458.3326	9.22356	
$a_1$	-39.6073	6.8765	
$a_2$	-10.2378	1.9838	
$a_3$	1.5039	0.5739	
$a_4$	-0.2776	0.1128	
$a_5$	0.091	3.52E-03	
$b_0$	36.7673	0.5783	
$b_1$	1.0328	0.1383	
$b_2$	3.95E-03	0.00683	
Reduced Chi	3.97E-05		
Adj. R-Square	0.9999		

Figure S19 C<sub>2</sub>H<sub>4</sub> isotherms (points) and Virial fitting curves (lines) of MOF-303 at 298 (red) and 273 K (blue).



Model		Isosteric heat	
Equation	$y = \ln(x) + 1/K * (a_0 + a_1 * x + a_2 * x^2 + a_3 * x^3 + a_4 * x^4 + a_5 * x^5) + (b_0 - b_1 * x + b_2 * x^2)$		
Temperature	273	298	
	value	Standard Error	
$a_0$	-2558.22256	8.1156	
$a_1$	-29.5783	5.7949	
$a_2$	-6.1393	1.9838	
$a_3$	1.0592	0.3763	
$a_4$	-0.1776	0.2864	
$a_5$	0.061	3.22E-03	
$b_0$	35.76832	0.5367	
$b_1$	1.0018	0.1277	
$b_2$	2.85E-03	0.00573	
Reduced Chi	3.97E-05		
Adj. R-Square	0.9999		

Figure S20 CO<sub>2</sub> isotherms (points) and Virial fitting curves (lines) of MIL-303 at 298 (red) and 273 K (blue).

**Table S3** The Langmuir parameter fits for the single component adsorption isotherms of C<sub>2</sub>H<sub>2</sub>, C<sub>2</sub>H<sub>4</sub> and CO<sub>2</sub> in MIL-160 at 298 K

	Site A	Site B	Site A	Site B
	q <sub>A,sat</sub> (mol kg <sup>-1</sup> )	b <sub>A</sub> (Pa <sup>-1</sup> )	q <sub>B,sat</sub> (mol kg <sup>-1</sup> )	b <sub>B</sub> (Pa <sup>-1</sup> )
C <sub>2</sub> H <sub>2</sub>	12.9	4.734E-05		
C <sub>2</sub> H <sub>4</sub>	4.4	2.093E-05	2.6	2.922E-05
CO <sub>2</sub>	7.4	1.800E-05		

**Table S4** The Langmuir parameter fits for the single component adsorption isotherms of C<sub>2</sub>H<sub>2</sub>, C<sub>2</sub>H<sub>4</sub> and CO<sub>2</sub> in MOF-303 at 298 K

	q <sub>sat</sub> (mol kg <sup>-1</sup> )	b (Pa <sup>-1</sup> )
C <sub>2</sub> H <sub>2</sub>	6.10196	2.48091
C <sub>2</sub> H <sub>4</sub>	4.38562	1.67162
CO <sub>2</sub>	5.6240	0.35165

#### S4. Molecular simulation

To gain a better insight into the adsorption behaviors of guests in MIL-160 and MOF-303, the Grand Canonical Monte Carlo (GCMC) simulations were performed in the Materials Studio 2017 [5]. The Crystallographic Information Files (CIFs) of MIL-160 and MOF-303 were downloaded from Cambridge Structural Database (CSD). The crystal structures were used in simulation process without further geometry optimization. The geometry of C<sub>2</sub>H<sub>2</sub>, C<sub>2</sub>H<sub>4</sub>, and CO<sub>2</sub> gas molecules were optimized in Forcite module. In order to obtain the atoms partial charge of MIL-160, MOF-303, C<sub>2</sub>H<sub>2</sub>, C<sub>2</sub>H<sub>4</sub> and CO<sub>2</sub>, QEq method and QEq\_neutral 1.0 parameter were applied and the convergence limit was set as  $5.0 \times 10^{-4}$ . Afterward, a series of simulations were conducted on adsorption model, applying the Metropolis method and Universal Force Field (UFF) in locate task. Edward & Group and Group-based were adopted as the summation method of electrostatic and van der Waals, respectively.

The CP2K code with quickstep module was performed to optimize the selected framework of the period structure of MIL-160 and MOF-303 [6], and the period Density Functional Theory (DFT) calculations were conducted by using the generalized gradient approximation (GGA) and the Perdew-Burke-Ernzerhof (PBE) functional, while the DFT-D3 was employed to accommodate the weak forces that might be present. Economic and suitable basis sets that Triple-plus valence polarized Gaussian-type (TZVP-MOLOPT-GTH) for C, H, O atoms and Double-plus valence polarization functions (DZVP-MOLOPT-SR-GTH) were used for Al atoms for the investigation of the adsorption energy. The self-consistent field (SCF) convergence value was set to  $5 \times 10^{-6}$  Hartree, while the energy cutoff of 350 Ry was used throughout the calculations. Adsorption energy ( $\Delta E$ ) was calculated by the following equation.

$$\Delta E = E_{Total} - (E_{MOF} + E_{gas}) \quad (S5)$$

Where  $E_{total}$ ,  $E_{MOF}$  and  $E_{gas}$  represent for the total systematic energy of MOF and adsorbate.

**Table S5** Partial charges (e) of atoms in different molecules

Molecules	C1	C2	O1	O2	H1	H2	H3	H4
C <sub>2</sub> H <sub>2</sub>	-0.133	-0.133	-	-	0.133	0.133	-	-
CO <sub>2</sub>	0.266	-	-0.133	-0.133	-	-	-	-
C <sub>2</sub> H <sub>4</sub>	-0.266	-0.266	-	-	0.133	0.133	0.133	0.133

where e represents the elementary charge,  $e = 1.6022 \times 10^{-19}$  C.

**Table S6** Adsorption energy (kJ mol<sup>-1</sup>) of MIL-160 and MOF-303 for different gas molecules

MOFs	MIL-160	MOF-303
C <sub>2</sub> H <sub>2</sub>	35.8	33.1
CO <sub>2</sub>	28.9	30.2
C <sub>2</sub> H <sub>4</sub>	29.3	31.5

**Table S7** The interaction type and distance existing in C<sub>2</sub>H<sub>2</sub>@MIL-160 and C<sub>2</sub>H<sub>2</sub>@MOF-303

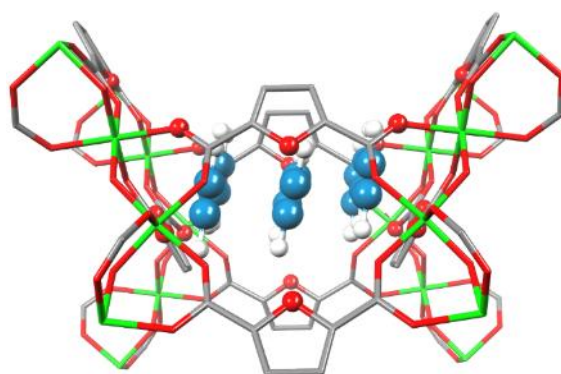
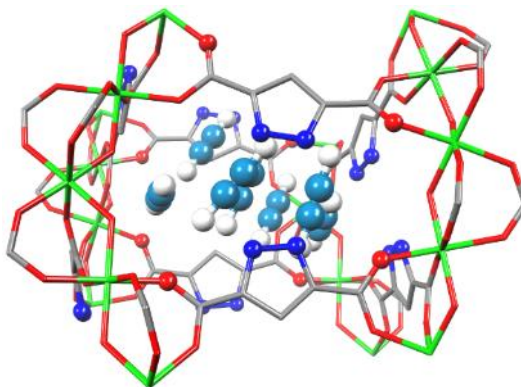
MOFs	Interaction types	Distance ranges (Å)
MIL-160	H-C≡C-H <sup>δ+</sup> ...O <sup>δ-</sup>	2.819 - 3.828
	H-C≡C-H <sup>δ+</sup> ...C <sup>δ-</sup>	2.981 - 3.363
	H-C≡C-H...π	3.278 - 3.398
MOF-303	H-C≡C-H <sup>δ+</sup> ...O <sup>δ-</sup>	3.226 - 3.932
	H-C≡C-H <sup>δ+</sup> ...C <sup>δ-</sup>	3.052 - 3.681
	H-C≡C-H...N	3.296 - 3.991
	H-C≡C-H...π	3.361 - 3.538

**Table S8** The interaction type and distance existing in CO<sub>2</sub>@MIL-160 and CO<sub>2</sub>@MOF-303

MOFs	Interaction types	Distance ranges (Å)
MIL-160	H-C≡C-H...π	3.413 - 3.901
MOF-303	H-C≡C-H...π	3.439 - 3.832

**Table S9** The interaction type and distance existing in  $C_2H_4@MIL-160$  and  $C_2H_4@MOF-303$ 

MOFs	Interaction types	Distance ranges (Å)
MIL-160	$H-C=C-H\delta+\cdots O\delta-$	3.322 - 3.983
	$H-C=C-H\cdots\pi$	3.472 - 3.898
MOF-303	$H-C=C-H\cdots N$	3.301 - 3.931
	$H-C=C-H\cdots\pi$	3.406 - 3.863

**Figure S21** The calculated binding configuration of  $C_2H_2@MIL-160$ .**Figure S22** The calculated binding configuration of  $C_2H_2@MOF-303$ .

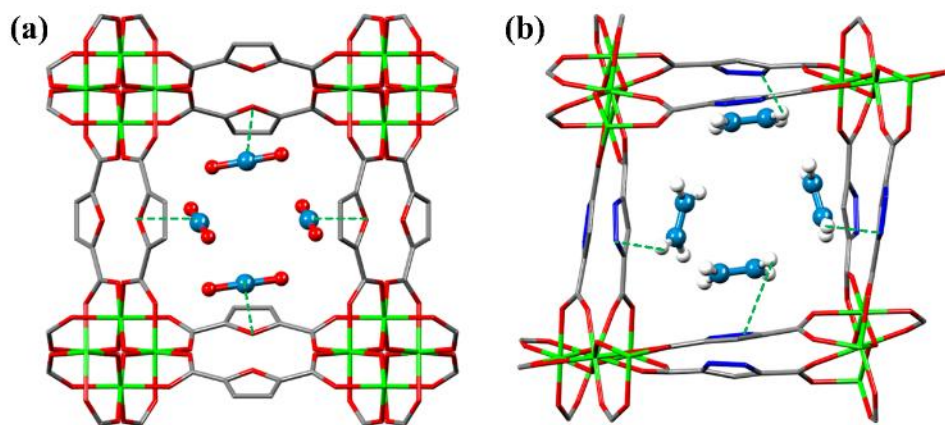


**Figure S23** The calculated binding configurations of (a) CO<sub>2</sub>@MIL-160 and (b) C<sub>2</sub>H<sub>4</sub>@MOF-303.

## S5. Breakthrough experiment

Breakthrough simulations: The performance of industrial fixed bed adsorbers is dictated by a combination of adsorption selectivity and uptake capacity. Transient breakthrough simulations were carried using the methodology described in earlier publications [7-11]. Two different feed mixtures were examined: 50/50 C<sub>2</sub>H<sub>2</sub>/CO<sub>2</sub> mixtures operating at a total pressure of 100 kPa, and temperatures of 298 K, 50/50 C<sub>2</sub>H<sub>2</sub>/C<sub>2</sub>H<sub>4</sub> mixtures operating at a total pressure of 100 kPa, and temperatures of 298 K. In these simulations, intra-crystalline diffusion influences are ignored. We choose length of packed bed,  $L = 0.3$  m, superficial gas velocity at the entrance to the bed,  $u_0 = 0.04$  m s<sup>-1</sup>; voidage of the packed bed,  $\varepsilon = 0.4$ . The

interstitial gas velocity  $v = \frac{u}{\varepsilon}$ . For presenting the breakthrough simulation results, the y-axis is the dimensionless concentrations of each component at the exit of the fixed bed, normalized with respect to the inlet feed concentrations. The x-axis is the dimensionless time,

$$\tau = \frac{tu}{L\varepsilon} \quad (S6)$$

For the desorption phase of C<sub>2</sub>H<sub>2</sub>/CO<sub>2</sub> mixtures, the simulations were performed with reported method [12].

The experimental breakthrough tests were operated at 298 K and 1.0 bar on a dynamic breakthrough instrument (Hidden QGA quantitative gas analysis system) The 50/50 C<sub>2</sub>H<sub>2</sub>/C<sub>2</sub>H<sub>4</sub> and C<sub>2</sub>H<sub>2</sub>/CO<sub>2</sub> were pre-mixed in gas pipeline with a flow rate of 2.0 mL min<sup>-1</sup>. A stainless-steel column (4.6 mm inner diameter × 50 mm) packed with MOF powders (0.51 and 0.49 g for MIL-160 and MOF-303) was activated by purging a constant He flow with a rate of 5 mL min<sup>-1</sup> at 393 K for 6 hours. Before each cyclic experiment, the sample was activated by heating at 393 K for 6 hours under He flow. The complete breakthrough of C<sub>2</sub>H<sub>2</sub> gas was monitored by the downstream gas composition reaching that of the feed gas. On the basis of the mass balance, the gas adsorption capacities can be determined as follows:

$$Q_i = \frac{v \times V\%}{22.4 \times m} \int_{t_0}^{t_1} (c_0 - c_i) dt \quad (S7)$$

where  $Q_i$  is the equilibrium adsorption capacity of gas  $i$  (mmol g<sup>-1</sup>),  $c_i$  is the feed gas concentration,  $v$  is the volumetric feed flow rate (mL min<sup>-1</sup>),  $V\%$  represents the molar fraction of CO<sub>2</sub> or C<sub>2</sub>H<sub>4</sub>.  $t_0$  and  $t_1$  are the initial and final adsorption time (min),  $c_0$  and  $c_i$  are the inlet and outlet gas concentration, respectively, and  $m$  is the mass of the adsorbent (g).



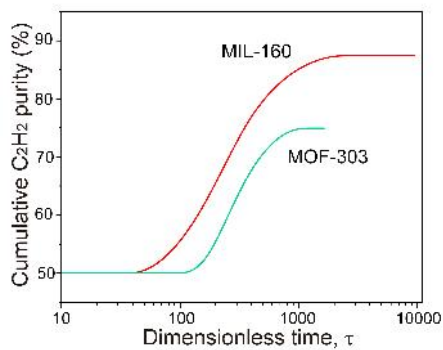


**Figure S24** Cumulative purity of  $C_2H_2$  recovered from MIL-160 and MOF-303 during simulated counter-current blowdown operations.

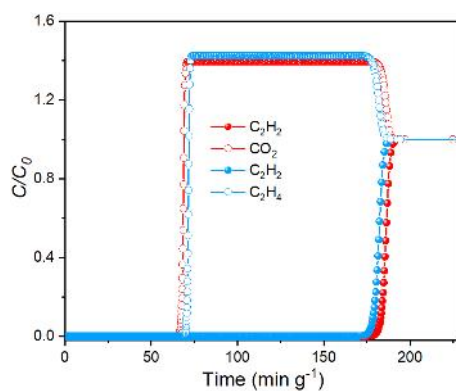


**Figure S25** Simulated breakthrough curves of equimolar  $C_2H_2/CO_2$  and  $C_2H_2/C_2H_4$  mixtures in MIL-160 at 298 K and 1.0 bar with a flow rate of 2.0

$mL\ min^{-1}$ .

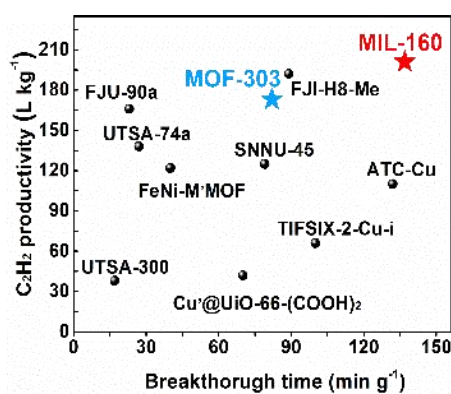


**Figure S26** The comparison of separation performances for equimolar  $C_2H_2/CO_2$  mixture on various MOFs with the same gas flow rate of 2 mL

$min^{-1}$  at 298 K.

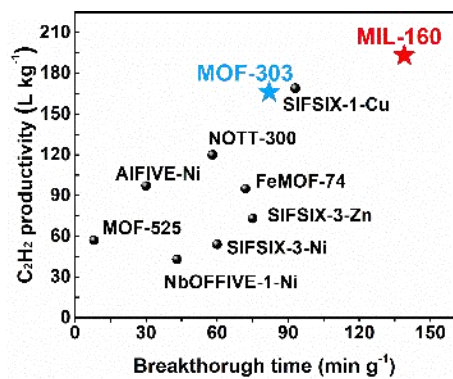


**Figure S27** The comparison of separation performances for equimolar  $C_2H_2/C_2H_4$  mixture on various MOFs with the same gas flow rate of 2 mL

$min^{-1}$  at 298 K.

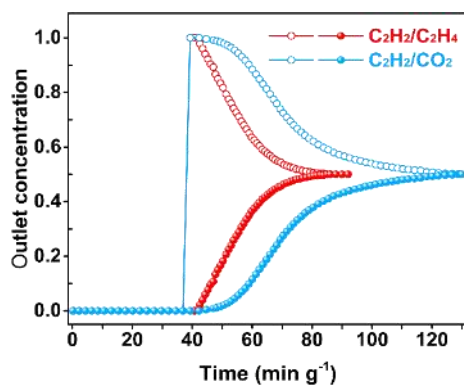


**Figure S28** The breakthrough curves of CAU-10-H for  $C_2H_2/C_2H_4$  and  $C_2H_2/CO_2$  mixtures (50/50) with flow rate of 2 mL  $min^{-1}$  at 298 K and 1.0 bar.

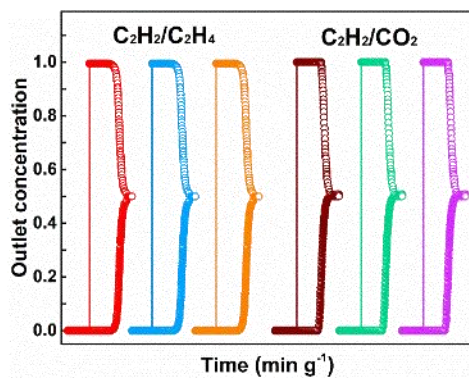


**Figure S29** Cyclic breakthrough experiment of  $C_2H_2/C_2H_4$  (50/50) and  $C_2H_2/CO_2$  (50/50) mixtures for MIL-160 at 298 K and 1.0 bar.

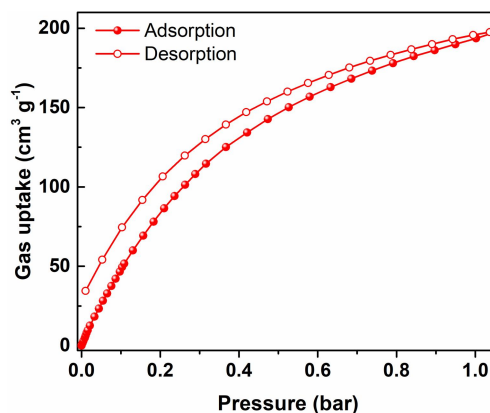


Figure S30 The isotherms of  $C_2H_2$  at 298 K on MIL-160 synthesized by hydrothermal method.

- [1] Xiang, S.;Zhou, W.;Gallegos, J. M.;Liu, Y.; Chen, B. Exceptionally High Acetylene Uptake in a Microporous Metal–Organic Framework with Open Metal Sites. *J. Am. Chem. Soc.* **2009**, *131*, 12415-12419.
- [2] Foo, M. L.;Matsuda, R.;Hijikata, Y.;Krishna, R.;Sato, H.;Horike, S.;Hori, A.;Duan, J.;Sato, Y.;Kubota, Y.;Takata, M.; Kitagawa, S. An Adsorbate Discriminatory Gate Effect in a Flexible Porous Coordination Polymer for Selective Adsorption of  $CO_2$  over  $C_2H_2$ . *J. Am. Chem. Soc.* **2016**, *138*, 3022-3030.
- [3] Solovyeva, M.;Krivosheeva, I.;Gordeeva, L.; Aristov, Y. MIL-160 as an Adsorbent for Atmospheric Water Harvesting. *Energies* **2021**, *14*, 3586.
- [4] Fathieh, F.;Kalmutzki, M. J.;Kapustin, E. A.;Waller, P. J.;Yang, J.; Yaghi, O. M. Practical water production from desert air. *Sci. Adv.*, *4*, eaat3198.
- [5] Metropolis, N.;Rosenbluth, A. W.;Rosenbluth, M. N.;Teller, A. H.; Teller, E. Equation of State Calculations by Fast Computing Machines. *J.Chem.* **1953**, *21*, 1087-1092.
- [6] Doerr, S.;Majewski, M.;Pérez, A.;Krämer, A.;Clementi, C.;Noe, F.;Giorgino, T.; De Fabritiis, G. TorchMD: A Deep Learning Framework for Molecular Simulations. *J. Chem. Theo.Comput.***2021**, *17*, 2355-2363.
- [7] Krishna, R. Methodologies for screening and selection of crystalline microporous materials in mixture separations. *Sep. Purif. Technol.* **2018**, *194*, 281-300.
- [8] Krishna, R. Metrics for evaluation and screening of metal–organic frameworks for applications in mixture separations. *ACS omega* **2020**, *5*, 16987-17004.
- [9] Krishna, R. The Maxwell–Stefan description of mixture diffusion in nanoporous crystalline materials. *Microporous Mesoporous Mater.* **2014**, *185*, 30-50.
- [10] Krishna, R. Methodologies for evaluation of metal–organic frameworks in separation applications. *RSC Advances* **2015**, *5*, 52269-52295.
- [11] Krishna, R. Screening metal–organic frameworks for mixture separations in fixed-bed adsorbers using a combined selectivity/capacity metric. *RSC Advances* **2017**, *7*, 35724-35737.
- [12] Wang, L.;Sun, W.;Zhang, Y.;Xu, N.;Krishna, R.;Hu, J.;Jiang, Y.;He, Y.; Xing, H. Interpenetration symmetry control within ultramicroporous robust boron cluster hybrid MOFs for benchmark purification of acetylene from carbon dioxide. *Angew. Chem. Int. Ed.* **2021**, *60*, 22865-22870.